Optimized Quantum Error Correction Codes for Experiments

V. Nebendahl
*Institut für Theoretische Physik, Universität Innsbruck, Technikerstr. 25, A-6020 Innsbruck, Austria**

We identify gauge freedoms in quantum error correction (QEC) codes and introduce strategies for optimal control algorithms to find the gauges which allow the easiest experimental realization. Hereby, the optimal gauge depends on the underlying physical system and the available means to manipulate it. The final goal is to obtain optimal decompositions of QEC codes into elementary operations which can be realized with high experimental fidelities. In the first part of this paper, this subject is studied in a general fashion, while in the second part, a system of trapped ions is treated as a concrete example. A detailed optimization algorithm is explained and various decompositions are presented for the three qubit code, the five qubit code, and the seven qubit Steane code.

arXiv:1411.1779v2 [quant-ph] 5 Mar 2015

Contents

I. Introduction 1

II. Quantum error correction 2
A. Degrees of freedom in QEC 2
1. Measuring the error syndrome 3
B. Fault-tolerance 4
C. Operations on logical qubits 4

III. Performance function 4
A. Error syndrome 5
B. Coherent QEC 6
C. Quantum gates on logical qubits 6
D. Evaluating the performance function 6

IV. Results 7
A. Three qubit code 8
B. Five qubit code and Steane code 8
1. State preparation for logical qubits 9
2. Stabilizer 10
3. Logical gates 12

V. Conclusion 13

VI. Acknowledgments 13

References 14

A. Elementary operations for trapped ions 14

B. Optimization algorithm for trapped ions 15
1. Extra criteria 15
a. First criterion 15
b. Second criterion 15
2. Optimization 15
a. First criterion 16
b. Second criterion 16
c. Simulated annealing 17
3. Protocols 17
a. Disturbing the sequence 17

*Electronic address: Volckmar.Nebendahl@uibk.ac.at

I. INTRODUCTION

Similar as their classical counterparts, complex quantum algorithms can be decomposed into sequences of elementary operations [1]. These decompositions are not unique and depending on the purpose, some of them might be better suited than others. In theoretical treatments for instance, the elementary operations used for decompositions are generally of such kind that they are as intuitive as possible. For experimental realizations on the other hand, it is an obvious approach to pick the elementary operations according to the available physical processes in the quantum system of choice such that it can be manipulated with the highest possible fidelity. As long as the elementary operations allow us to assemble a universal set of quantum gates, the existence of decompositions based on these operation is guaranteed for arbitrary quantum algorithms [2]. Still, in this paper we are not just interested in the mere existence of such decompositions, but seek ways to find decompositions which are as close to optimal as possible. In particular, we focus on quantum error correction codes, as well as operations on logical qubits encoded in error protected states.

As explained in more detail below, these types of codes (respectively algorithms) are equipped with different kinds of gauge invariances, which offer greater freedom when we intend to decompose them. We are no longer constrained to find a perfect one-to-one match. It suffices to find a sequence of elementary operations which reproduces the given code up to a gauge transformation. This increases the number of acceptable solutions and with that the probability to find better sequences, which allow high experimental fidelities.

To understand the origin of the quantum errpor correction (QEC) gauge freedom we are interested in, we have to remind ourselves that errors increase the entropy of a quantum system. QEC codes remove these errors and thereby reduce the entropy. Since entropy can only be reduced locally but not globally, one always needs to include a process which maps the information of the error onto another system to balance the entropy. This mapping is not unique and due to this lack of uniqueness, each QEC code contains an inherent gauge freedom. Of course, these mappings are subjected to constraints, but

we are still left with some degrees of freedom we can exploit.

For logical operations on error protected logical qubits, on the other hand, the objective is that a correctable error is not amplified under these logical operations, but it may still be mapped onto any other correctable error. The freedom contained in this mapping can be exploited, too.

Still, having identified these extra degrees of freedom does not imply that we can harness them. Finding an optimal decomposition is a non trivial task and it is advisable to seek the help of a (classical) computer. Except for the gauge freedom, this is a typical task for optimal control theory, which has already been applied successfully to various different quantum systems [3]. Therefore, a central concern of this paper is to show how the above identified gauge freedoms can be integrated in an optimal control algorithm.

Many of the ideas presented in this paper are of a general nature and device independent, while on the other hand any specific decomposition depends on the underlying quantum system. This dichotomy between generality and peculiarity is also reflected by the setup of this paper. In the first part, general aspects are treated which are common to all quantum systems, while the results presented in Sec. IV focus on a specific system consisting of trapped ions [4].

In more detail, the structure of the paper is the following: In Sec. II, the different kinds of gauge freedoms are worked out. Sec. III outlines how these gauge freedoms translate into an optimal control algorithm. In the Results section (Sec. IV), various decompositions are shown, comprising the three qubit code [5], the five qubit code [6], and the seven qubit Steane code [7]. The algorithm used to obtain these results is explained in detail in Appendix B).

II. QUANTUM ERROR CORRECTION

In this paper, we are mainly interested in experimental realizable QEC codes, which favor simple approaches. Hence, the needed theoretical background is quite limited and can be found, e.g., in Ref. [2].

The QEC codes we are interested in all define two codewords, $|0_L\rangle$ and $|1_L\rangle$, to which we also refer as the logical states. With them, an error protected logical qubit state $|\psi_L\rangle$ can be defined as

$$|\psi_L\rangle = \alpha \cdot |0_L\rangle + \beta \cdot |1_L\rangle \quad \text{with} \quad |\alpha|^2 + |\beta|^2 = 1. \quad (1)$$

The logical states $|0_L\rangle$ and $|1_L\rangle$ describe two states in a higher-dimensional Hilbert space, which is given as the product space of several single qubits, to which we refer as the physical qubits.

The logical states are chosen such that even after the occurrence of certain errors E_j, the logical qubit state $|\psi_L\rangle$ (1) can still be reconstructed by an error correcting code

$$E_j \cdot |\psi_L\rangle \xrightarrow{\text{QEC}} |\psi_L\rangle. \quad (2)$$

Different QEC codes define different codewords for the logical states $|0_L\rangle$ and $|1_L\rangle$ and allow for different errors to be corrected. Further, the choice of the codewords influences the way logical gates U_L, which operate on logical qubits $|\psi_L\rangle$, have to be realized on the level of the physical qubits.

In this paper, we are interested in finding the simplest possible experimental realization of logical gates and quantum error correction based on given codewords $|0_L\rangle$ and $|1_L\rangle$. That is, our aim is not to invent new QEC codes with new codewords, but to find variations of already existing codes.

A. Degrees of freedom in QEC

Probably the simplest example for a QEC code is the three qubit code [5], where the codewords for the logical qubit states $|0_L\rangle$ and $|1_L\rangle$ consist of three physical qubits,

$$|0_L\rangle = |000\rangle \text{ and } |1_L\rangle = |111\rangle. \quad (3)$$

This encoding allows us to identify and correct a single bit-flip error on any of the three physical qubits. A possible way to identify such an error is to measure the physical qubits and use a majority vote, but these measurements would also destroy the quantum information stored in the logical qubit $|\psi_L\rangle$ (1). This problem can be avoided if the information about the error is mapped onto auxiliary qubits. Subsequently, the information in the auxiliary qubits (the error syndrome) can either be measured or used coherently to correct the error. Fig. 1 shows a possible circuit for a coherent error correction. After the error is corrected, the logical qubit is once again disentangled from the auxiliary qubits, whose final state is of no further interest. In Fig. 1, this is symbolized by the arbitrary unitary gate U operating on the auxiliary qubits at the end of the circuit. This unitary gate U can be seen as a gauge transformation – it changes the code, but it does not change the result of the error correction on the logical qubit. Due to this gauge freedom, we do not just have one bit-flip error correcting QEC code but an entire equivalence class.

Of course, simply adding such a unitary operator at the end of an already perfectly working QEC is of no advantage at all. But we have to remember the task we are facing: We are not looking for a decomposition of the QEC code in terms of the standard gates used in Fig. 1, but for the simplest decomposition in operations which are tailored for the quantum system we are using. In this search, it is a great difference whether we have just one solution which we are allowed to accept or an entire equivalence class of correct solutions.

1. Measuring the error syndrome

Now, we turn to QEC codes which incorporate measurements of the auxiliary qubits to determine the error syndrome. In the case of the three qubit code example a bit-flip error can be identified using the quantum circuit shown in Fig. 2. The possible measurement outcomes (00), (01), (10), and (11) correspond to the four cases: no error, bit-flip on the first physical qubit, bit-flip on the second physical qubit, and bit-flip on the third physical qubit. Here, we face a fixed mapping between the measurement results and the error. Hence, the situation is different compared to the measurement-free example above, where we did not care for the final state of the auxiliary qubits.

Nonetheless, we can still consider alternative mappings. But if we do so, we have to make sure that these mappings are unambiguous, i.e., it is not enough that the different measurement results correspond to orthogonal error states, but one also has to avoid measurement results which correspond to superpositions of errors, since otherwise the correction operation would be ill defined. As long as we take care of this, we can even allow codes which change the error on the logical qubit, as long as the error maintains correctable.

Such alternative mappings cause no problems if we choose them by hand. But we are looking for degrees of freedom which can be manipulated by the computer itself in the attempt to find optimal decompositions. If we try to let the computer find the best mapping, we have to make sure that the above-mentioned side conditions are fulfilled, which causes the optimization problem to become much more involved. A further difficulty arises for optimization problems which are so complex that we have to split them into several smaller problems (e.g., stabilizer codes, where the code for each stabilizer might be computed separately; see Sec. IV B 2). If we allow the computer to alter the mapping in such a case, this change has to be synchronized for all subprocesses. Since these subprocesses can no longer be handled independently, splitting a complex problem into smaller subprocesses might not result in the intended simplification of the problem at all. But there are also some mappings which entail none of the above mentioned problems. These mappings, we are going to study next.

First, let us define the following symbols

$$\begin{array}{rl} E_j & \text{elementary correctable error} \\ |0_L\rangle, |1_L\rangle & \text{basis of the logical qubit} \\ |0_A\rangle & \text{inital state of the auxiliary qubits} \\ |e_j\rangle & \text{final state of the auxiliary qubits corresponding to the error } E_j. \end{array} \tag{4}$$

The E_j form a minimal basis of operators for all correctable errors (i.e. $\alpha \cdot E_i + \beta \cdot E_j$ is a correctable error while $E_i \cdot E_j$ is generally not), including the identity. Each E_j corresponds to exactly one possible measurement result $|e_j\rangle$ of the auxiliary qubits.

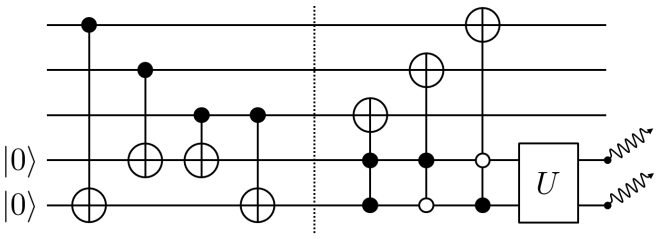

Figure 1: Example circuit for the three qubit quantum error correction code without measurement. The top three horizontal lines represent the physical qubits used to encode the logical qubit, while the two horizontal lines at the bottom represent two auxiliary qubits. The dotted vertical line was included to separate the two functional parts of the code: The part to the left of the dotted line maps the information of a possible bit-flip error onto the auxiliary qubits. The part on the righjt uses this information to correct the error. After the error is corrected, the state of the auxiliary qubits is of no further interest and might be reset (wavy line) for the next run. Therefore, an arbitrary unitary operation U on the auxiliary system can be included.

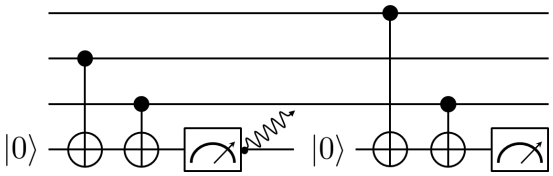

Figure 2: Example circuit for a three qubit quantum error correction code based on measurement. As in Fig. 1, the top three lines represent the physical qubits used to encode the logical qubit, while the bottom line represents an auxiliary qubit. After the first measurement, the auxiliary qubit is reset to reuse it for the second measurement. The measurement results (00), (01), (10), and (11) correspond to the four cases: no error, bit-flip on the first qubit, bit-flip on the second qubit and bit-flip on the third qubit.

To identify the error, we need a unitary operator $U_{\text{Syn.}}$ which calculates the error syndrome, i.e. $U_{\text{Syn.}}$ maps the error E_j onto the auxiliary qubits $|0_A\rangle \to |e_j\rangle$, while the logical qubit stays unchanged. The most general form for such an operator $U_{\text{Syn.}}$ is given by

$$\begin{aligned} U_{\text{Syn.}} = &\sum_j e^{i\varphi_j} E_j \left(|0_L\rangle\langle 0_L| + |1_L\rangle\langle 1_L|\right) E_j^\dagger \otimes |e_j\rangle\langle 0_A| \\ &+ M_C \end{aligned} \tag{5}$$

with arbitrary phases φ_j. Here, $|0_L\rangle\langle 0_L| + |1_L\rangle\langle 1_L|$ is the identity in the Hilbert space of the logical qubits, but it is *not* an identity in the Hilbert space of the physical qubits, where the error occurs. Further, we added M_C in Eq. (5) for formal reasons only, i.e. to complement $U_{\text{Syn.}}$ to a unitary operator. M_C operates exclusively on states which are in the kernel of the operator sum in the first line of Eq. (5), as, e.g., input states where the auxiliary qubits are not initialized. Apart from the unitarity constraint of $U_{\text{Syn.}}$, the operator M_C is completely arbitrary.

In textbook decompositions of $U_{\mathrm{Syn.}}$ (5), the phase factors $e^{i\varphi_j}$ are usually set to $e^{i\varphi_j} = 1$, but φ_j can also adopt any other value, without effecting the result of the error correction. The phase factors $e^{i\varphi_j}$ introduce relative phases between the superposition branches belonging to different elementary errors. Since all QEC codes are designed such that only one of these elementary errors survives after the measurements [2], the remaining phase solely adds to the global phase and hence does no harm [21].

B. Fault-tolerance

The optimization algorithm we will derive in this paper is designed to find a suitable sequence of technically feasible elementary operations such that the collective action of this sequence is identical to the effect of a given QEC code. For practical reasons, this is all we will demand, but from the theoretical point of view, one might demand more. To comply with the paradigm of the fault-tolerant quantum computation [2, 8, 9], we also would have to ensure that a single error occurring during the execution of the sequence does not result in the total loss of a formerly error-free logical qubit (or at least, the probability of a total loss has to be sufficiently small). Evidently, including such an extra demand would complicate the optimization task, but it would also impose constraints upon the selection of the elementary operations. For example, it is hard to conceive a fault-tolerant sequence based on elementary operations which corrupt many qubits at once in the case of a single error. In total, the demand for fault tolerance might hinder us to find any practical solution at all. Thus, we adopt a pragmatical point of view: As long as the experimental capacities to realize quantum error correction are still far behind the theoretical visions, it seems more important to provide experimentally realizable code than to have all theoretical aspects covered. Therefore, we feel safe to ignore some demands of fault tolerance for the time being and postpone their solution into the future.

Nonetheless, we will not sacrifice all ideas of fault tolerance. Beside the ability to correct errors, we also need to be able to apply logical operators (quantum gates) on logical qubits. We still demand that correctable errors (which are already present before the logical operators are applied) are not amplifies by these logical operators.

C. Operations on logical qubits

Here, we restrict ourselves to logical operators which act on a single logical qubit only. In order to avoid error amplification, we could demand that any logical operator $\hat{O}$ has to commutate with any correctable error E_j, when applied to an arbitrary logical qubit $|\psi_L\rangle$, i.e., $\hat{O}\cdot E_j|\psi_L\rangle = E_j\cdot\hat{O}|\psi_L\rangle$. But this is more than needed. It suffices that under any logical operation $\hat{O}$ correctable errors are only allowed to transform into other correctable errors, i.e.,

$$\hat{O}\cdot E_j|\psi_L\rangle = \sum_k \alpha_{jk}\cdot E_j\cdot\hat{O}|\psi_L\rangle, \quad \sum_k |\alpha_{jk}|^2 = 1, \tag{6}$$

with the extra degree of freedom to adopt the α_{jk}.

On the other hand, we have to remember that the identity operation is part of the elementary errors $\{E_j\}$, as well. That is, although Eq. (6) avoids error amplification, it allows that an error-free state is mapped onto an incorrect (but still correctable) result. To prevent this from happening, it is advisable to introduce a hierarchy of correctable errors and to distinguish at least the hierarchy levels "zero incorrect qubits" and "one incorrect qubit." For more advanced codes, further levels might be added. With that, we demand that errors are only mapped onto errors of the same hierarchy level. Using the index h to enumerate the hierarchy levels and denoting the errors by E_{h,j_h}, this demand can be formulated as

$$\hat{O}\cdot E_{h,j_h}|l\rangle = \sum_{k_h} \alpha_{j_h k_h}\cdot E_{h,k_h}\hat{O}|\psi_L\rangle, \ \sum_{k_h}|\alpha_{j_h k_h}|^2 = 1. \tag{7}$$

At a first glance, one might also want to accept the case where some errors are reduced due the application of the operator $\hat{O}$, but this is ruled out by entropy if we do not allow error accumulation elsewhere for compensation.

III. PERFORMANCE FUNCTION

After having introduced the different degrees of freedom we intend to use, we have to investigate how they are integrated into the optimization routine.

We like to optimize QEC codes in the circuit model of quantum computation. These codes might consist of several components, as, e.g., unitary operations which map an error syndrome onto some auxiliary qubits followed by a measurement and finally an active correction of the error according to the measurement results [2]. The measurement and the active correction are usually elementary operations and considered as trivial in this context. The only part we intend to optimize are the complex unitary operations.

Any unitary operator U has to be built up using some elementary operations $u_t(\alpha_t)$ which can be generated in the laboratory,

$$U = U(\boldsymbol{\alpha}) = \prod_t u_t(\alpha_t). \tag{8}$$

The origin of this decomposition (8) depends on the treatment of the quantum system in question. The $u_t(\alpha_t)$ might represent some effective unitaries which can be generated easily and with high fidelity. This is, e.g., the case for the second part of this paper, where we demonstrate the ideas for trapped ions. Alternatively,

the $u_t(\alpha_t)$ might result from the necessity to discretize the general time ordered equation

$$U = \mathcal{T} \exp\left(-\frac{i}{\hbar}\int_0^T dt \cdot H\left(\alpha(t)\right)\right) \tag{9}$$

to treat it numerically. Depending on the situation, each α_t either stands for a single control parameter or represents an entire set of such parameters, $\alpha_t \equiv \alpha_{t,j}$. In either case, these are the parameters we have to optimize.

How is this optimization done? Let us start with a simple example. Suppose we like to generate the operator U_{target}. As a first step, we define the real valued performance function $\Phi_{\text{Re}}(\boldsymbol{\alpha})$,

$$\begin{aligned}\Phi_{\text{Re}}(\boldsymbol{\alpha}) &:= \text{Re}(\langle U_{\text{target}}| \prod_t u_t(\alpha_t)\rangle) \\ &= \text{Re}(\text{tr}(U_{\text{target}}^\dagger \cdot \prod_t u_t(\alpha_t))).\end{aligned} \tag{10}$$

This function reaches its maximum if and only if

$$\prod u_t(\alpha_t) = U_{\text{target}}. \tag{11}$$

In principal, we could now use a standard optimization procedure as, e.g., a gradient ascent algorithm [10, 11] to find solutions for the α_t. Therefore, we consider this example problem as solved.

Next, suppose we take the absolute value in Eq. (10) instead of the real value,

$$\Phi_{\text{Abs}}(\boldsymbol{\alpha}) := |\langle U_{\text{target}}| \prod_t u_t(\alpha_t)\rangle|^2. \tag{12}$$

This performance function is now maximized by all $\boldsymbol{\alpha}$ with

$$\prod u_t(\alpha_t) = e^{i\varphi} \cdot U_{\text{target}}. \tag{13}$$

In case we can tolerate the extra phase factor $\exp(i\varphi)$, $\Phi_{\text{Abs}}(\boldsymbol{\alpha})$ (12) defines the preferable performance function since it exploits an extra degree of freedom and accepts more solutions. Here, we get a first idea how the degrees of freedom found for QEC codes in Sec. II might be used.

A. Error syndrome

Now, let us construct a performance function which is maximal if $\prod u_t(\alpha_t)$ equals any of the $U_{\text{Syn.}}$ described in Eq. (5). It might be helpful to keep in mind that the performance function is just a mathematical tool, which helps us to find the correct α_t. It does not need to have a meaningful physical interpretation.

First, we make the obvious choice not to include the unimportant part M_C (5) into the performance function. M_C acts exclusively on states we are not interested in and was only introduced for the formal reason to make $U_{\text{Syn.}}$ unitary. Dropping it reduces the class of adequate unitaries $U_{\text{Syn.}}$ to a class of projectors with elements $P_{\text{Syn.}}$,

$$\begin{aligned}P_{\text{Syn.}} &= \sum_j e^{i\varphi_j} E_j \left(|0_L\rangle\langle 0_L| + |1_L\rangle\langle 1_L|\right) E_j^\dagger \otimes |e_j\rangle\langle 0_A| \\ &= \sum_j \sum_{l=1}^{2} e^{i\varphi_j} \cdot E_j |l_L\rangle\langle l_L| E_j^\dagger \otimes |e_j\rangle\langle 0_A|\end{aligned} \tag{14}$$

Next, we introduce the double indexed object p_{lj} as

$$p_{lj} = E_j |l_L\rangle\langle l_L| E_j^\dagger \otimes |e_j\rangle\langle 0_A|, \quad l = 0, 1. \tag{15}$$

As can be easily checked, $P_{\text{Syn.}} = \sum_{lj} e^{i\varphi_j} \cdot p_{lj}$.

The p_{lj} are fixed and known objects with no further degree of freedom. To avoid confusions, we emphasize that the objects p_{lj} are operators, but contrary to common notations the indices l, j do not enumerate bra and ket bases, i.e., $\hat{p} \neq p_{lj} \cdot |l\rangle\langle j|$.

Now, as a first (and insufficient) attempt, one might try the performance function

$$\begin{aligned}\Phi_{\text{try}}(\boldsymbol{\alpha}) &= \sum_{lj} \left|\langle p_{lj}| \prod_t u_t(\alpha_t)\rangle\right|^2 \\ &= \sum_{lj} \left|\text{tr}(p_{lj}^\dagger \cdot \prod_t u_t(\alpha_t))\right|^2.\end{aligned} \tag{16}$$

This performance function is maximal, if all summands $|\text{tr}(p_{lj}^\dagger \cdot \prod_t u_t(\alpha_t))|$ are maximal. That is, $\Phi_{\text{try}}(\boldsymbol{\alpha})$ is maximized, if

$$\text{tr}(p_{lj}^\dagger \cdot \prod_t u_t(\alpha_t)) = e^{i\varphi_{lj}}, \tag{17}$$

for all l, j. The problem with this performance function is that the phases $e^{i\varphi_{lj}}$ for the logical states $|0_L\rangle$ and $|1_L\rangle$ are not synchronized, i.e. the performance function is maximized for all

$$\prod_t u_t(\alpha_t) = \sum_{lj} e^{i\varphi_{lj}} \cdot E_j |l_L\rangle\langle l_L| E_j^\dagger \otimes |e_j\rangle\langle 0_A| + M_C, \tag{18}$$

with phases φ_{lj} that depend on $|l\rangle$. This can be easily amended by summing over the index l *before* taking the absolute value,

$$\Phi_{\text{two sums}}(\boldsymbol{\alpha}) = \sum_j \left|\sum_l \langle p_{lj}| \prod_t u_t(\alpha_t)\rangle\right|^2. \tag{19}$$

The absolute square of the sum over $l = 0, 1$ generates three terms: $|\langle p_{0,j}| \prod_t u_t(\alpha_t)\rangle|^2$, $|\langle p_{1,j}| \prod_t u_t(\alpha_t)\rangle|^2$, and $\text{Re}\big(\langle p_{0,j}| \prod_t u_t(\alpha_t)\rangle \cdot \langle \prod_t u_t(\alpha_t)| p_{1,j}\rangle\big)$. A closer look reveals that it suffices to take only the last term into account, i.e. the final version of the performance function for the error syndrome becomes

$$\Phi(\boldsymbol{\alpha}) = \sum_j \text{Re}\Big(\langle p_{0,j}| \prod_t u_t(\alpha_t)\rangle \cdot \langle \prod_t u_t(\alpha_t)| p_{1,j}\rangle\Big), \tag{20}$$

which can only become maximal if $\langle p_{0,j}|\prod_t u_t(\alpha_t)\rangle = e^{i\varphi_j} = \langle p_{1,j}|\prod_t u_t(\alpha_t)\rangle$ (for each j).

By now, we have found a performance function $\Phi(\boldsymbol{\alpha})$ which allows us to optimize over all degrees of freedom we have identified for the unitary operation that maps the error onto the auxiliary qubits. The same approach can be used if we like to map a stabilizer [2, 12] onto an auxiliary qubit. For the coherent QEC approach without measurement (see the beginning of Sec. II) on the other hand, we need a new performance function. This is what we are constructing next.

B. Coherent QEC

First, we define a new double indexed object $\tilde{p}_{lj}$ as

$$\tilde{p}_{lj} = |l_L\rangle\langle l_L|E_j^\dagger \otimes \langle 0_A|, \quad l = 0, 1. \tag{21}$$

The input states (right or "bra" side) are the same as for p_{lj} (15) but the output states are different. Since the coherent QEC corrects the error, we find the error-free states $|l_L\rangle$ instead of $E_j|l_L\rangle$. Further, no output is determined into the Hilbert space of the auxiliary qubits, which corresponds to the freedom we have identified for this model. To see this more clearly, we have to look at

$$\begin{aligned}\langle\tilde{p}_{lj}|\prod_t u_t(\alpha_t)\rangle &= \mathrm{tr}(\tilde{p}_{lj}^\dagger \cdot \prod_t u_t(\alpha_t)) \\ &= (\langle l_L| \cdot \prod_t u_t(\alpha_t) \cdot E_j|l_L\rangle \otimes |0_A\rangle) \\ &= |a_{lj}\rangle. \end{aligned}\tag{22}$$

For fixed l, j, the ket vector $|a_{lj}\rangle$ describes a state in the Hilbert space of the auxiliary qubits with $\||a_{lj}\rangle\| \leq 1$. The value $\||a_{lj}\rangle\| = 1$ is only adopted iff the erroneous state $E_j|l_L\rangle$ is corrected to $|l_L\rangle$ by $\prod_t u_t(\alpha_t)$. Let us recapitulate what we know about the physical state of the auxiliary qubits after a successful coherent error correction: The state is allowed to be arbitrary, but of course it has to be normalized to one and the state has to be independent of the logical state $|l_L\rangle$, since otherwise the auxiliary qubits would be entangled with the logical qubit. All these conditions are met if the expression

$$\sum_j \mathrm{Re}(\langle a_{0,j}|a_{1,j}\rangle) \tag{23}$$

is maximized. With that, we obtain the performance function for the coherent QEC approach,

$$\tilde{\Phi}(\boldsymbol{\alpha}) = \sum_j \mathrm{Re}\Big(\langle\tilde{p}_{0,j}|\prod_t u_t(\alpha_t)\rangle \cdot \langle\prod_t u_t(\alpha_t)|\tilde{p}_{1,j}\rangle\Big). \tag{24}$$

C. Quantum gates on logical qubits

Finally, we turn to the performance function for quantum gates on logical qubits. In Sec. II C we demanded that any quantum gate $\hat{O}$ should map errors onto errors of the same level of hierarchy. The needed projectors for such mappings are given by

$$\hat{p}_{l,h,j_h,k_h} = E_{h,k_h} \cdot \hat{O}|l_L\rangle\langle l_L|E_{h,j_h}^\dagger, \tag{25}$$

where h denotes the hierarchy level. Except for the extra indices, the new performance function can be formulated with $\hat{p}_{h,j_h,k_h,l}$ using the same structure as for the two examples seen before (20) and (24)

$$\hat{\Phi}(\boldsymbol{\alpha}) = \sum_{h,j_h,k_h} \mathrm{Re}\Big(\langle\hat{p}_{0,h,j_h,k_h}|U(\boldsymbol{\alpha})\rangle \cdot \langle U(\boldsymbol{\alpha})|\hat{p}_{1,h,j_h,k_h}\rangle\Big), \tag{26}$$

with $U(\boldsymbol{\alpha}) = \prod_t u_t(\alpha_t)$. It might be helpful to compare this performance function to a version without the summation over k (i.e., $k = j$). Such a performance function is deprived of the freedom to alter the type of error. Still, due to the fact that $U(\boldsymbol{\alpha})$ is unitary, the maximal value of both performance functions is exactly the same – it is just not reached for so many $U(\boldsymbol{\alpha})$ if the summation over k is missing.

Remark: For the coherent QEC we omitted the ket basis for the auxiliary qubits in $\tilde{p}_{lj}$ (21). Alternatively, we could also have included a k-indexed basis followed by a summation over this index in the performance function.

D. Evaluating the performance function

In order to optimize the performance function, one needs to vary over the parameters α_t. This can be done in an efficient manner [10], as we are about to see for the derivatives $(\frac{\partial}{\partial\alpha_0}, \frac{\partial}{\partial\alpha_1}, \ldots, \frac{\partial}{\partial\alpha_T})$. To keep the demonstration simple, we treat each α_t as a single parameter, although it might also represent an entire set of parameters (see above).

For further convenience, we write p_{lj} (15) as

$$p_{lj} = |f_{lj}\rangle\langle i_{lj}|. \tag{27}$$

With that, the central element of the performance function (20) reads

$$\begin{aligned}\langle p_{lj}|\prod_{t=0}^{T} u_t(\alpha_t)\rangle &= \mathrm{tr}\langle p_{lj}^\dagger \cdot \prod_{t=0}^{T} u_t(\alpha_t)\rangle \\ &= \langle f_{lj}|\prod_{t=0}^{T} u_t(\alpha_t)|i_{lj}\rangle \end{aligned}\tag{28}$$

and its derivatives with respect to α_k become

$$\frac{\partial}{\partial\alpha_k}\langle\ldots\rangle = \langle f_{lj}|\prod_{t=0}^{k-1} u_t(\alpha_t) \cdot \frac{du_k(\alpha_k)}{d\alpha_k} \cdot \prod_{t=k+1}^{T} u_t(\alpha_t)|i_{lj}\rangle. \tag{29}$$

Since $\langle f_{lj}|\prod_{t=0}^{k-1} u_t(\alpha_t)$ and $\prod_{t=k+1}^{T} u_t(\alpha_t)|i_{lj}\rangle$ can be calculated iteratively for all k, the number of matrix multiplications needed to calculate *all* derivatives

$(\frac{\partial}{\partial\alpha_0},\ldots,\frac{\partial}{\partial\alpha_T})$ scales down from quadratic in n to linear in n, which allows e.g. an efficient application of a gradient ascent algorithm [10, 11].

IV. RESULTS

So far, the discussion was fairly general and independent of any specifications due to the chosen physical system. But these specifications are important to generate an optimal code. Therefore, we now make a choice and show the optimization results for a quantum system consisting of trapped ions [4]. Still, we do not need to delve deep into the physics of trapped ions. The only system dependent specification we need is a description of the elementary operations $u_t(\alpha_t)$ appearing in Eq. (8).

For trapped ions, we use effective unitaries as elementary operations, from which we know how to produce them with very high fidelities. The Hilbert space these effective unitaries operate on is entirely restricted to the Hilbert space of the qubits. The advantage of such an effective approach is a much simpler optimization task. The effective unitaries $u_t(\alpha_t)$ over which we optimize can be described by a set of effective N-qubit Hamiltonians H_j as

$$\begin{aligned} u_t(\alpha_t) &= \exp\left(-i\cdot\alpha_t\cdot H_{j_t}\right), \quad \text{with} \\ H_j &\in \{S_x^2, S_y^2, S_x, S_y, \sigma_z^{(1)}, \sigma_z^{(2)}, \ldots, \sigma_z^{(N)}\}, \\ S_{x/y} &= \tfrac{1}{2}\sum_{j=1}^{N}\sigma_{x/y}^{(j)}, \end{aligned} \tag{30}$$

where $\sigma_{x/y/z}^{(j)}$ denote Pauli matrices applied on the jth qubit. Linear combinations of the Hamiltonians are not allowed, which is e.g. in great contrast to the typical optimization task found in nuclear magnetic resonance (NMR) [10]. The $\exp(-i\cdot\alpha_t\cdot S_{x/y}^2)$ represent Mølmer-Sørensen gates [13]. They are the only entangling gates in this set and were chosen because they are currently the entangling gates with the highest fidelities [14]. More motivations for the specific choice of the $u_t(\alpha_t)$ in Eq. (30) are given in App. A.

To identify the effective unitaries $u_t(\alpha_t) = \exp(-i\cdot\alpha_t\cdot H_{\text{eff}}^{(t)})$, we need two pieces of information: α_t and $H_{\text{eff}}^{(t)}$. To this purpose, we use the following notation:

$$\begin{aligned} z_j(\Theta) &= \exp\big(-i\cdot\Theta\cdot\frac{\sigma_z^{(j)}}{2}\big) \\ X(\Theta) &= \exp(-i\cdot\Theta\cdot S_x) \\ Y(\Theta) &= \exp(-i\cdot\Theta\cdot S_y) \\ X^2(\Theta) &= \exp(-i\cdot\Theta\cdot S_x^2) \\ Y^2(\Theta) &= \exp(-i\cdot\Theta\cdot S_y^2), \end{aligned} \tag{31}$$

with $S_{x/y} = \frac{1}{2}\sum_{j=1}^{N}\sigma_{x/y}^{(j)}$. Further, we introduce the two

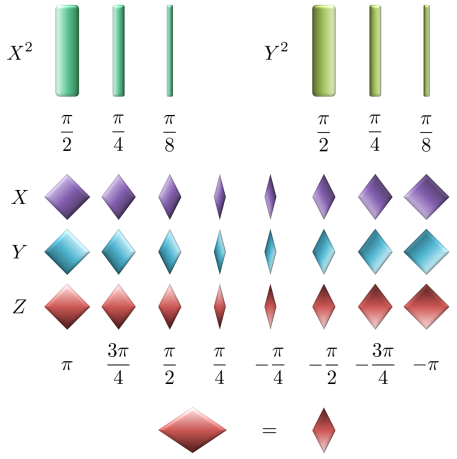

Figure 3: The symbols used for the graphical representation of $X(\Theta)$, $Y(\Theta)$, $z_j(\Theta)$, $X^2(\Theta)$, and $Y^2(\Theta)$ (31) in a quantum circuit. The width of the symbols is proportional to the absolute value of Θ, where the width belonging to $\Theta=\pi$ equals the vertical distance of the qubits in the quantum circuit. The symbols for the entangling Mølmer-Sørensen gates $X^2(\Theta)$ and $Y^2(\Theta)$ are extended over all qubits, while the symbols for the non-entangling collective operations $X(\Theta)$ and $Y(\Theta)$ are (vertically) repeated such that all qubits are covered. The symbol for the local $z_j(\Theta)$ is placed on the jth qubit only. Currently, $z_j(\Theta)$ with negative values for Θ are experimentally realized as $z_j(-|\Theta|) = z_j(2\pi - |\Theta|)$. Therefore, the symbols for negative z_j are replaced by their longer positive counterparts, as well.

symbols

$$\begin{aligned} M_j &: \text{measurement of } j\text{th qubit} \\ R_j &: \text{reset of } j\text{th qubit to } |1\rangle. \end{aligned} \tag{32}$$

Besides the mathematical transcription, each result is also given as graphical representation. Here, we follow the conventions used for quantum circuit: Qubits are depicted as horizontal lines and operators (gates) are given by symbols placed on the lines of the qubits in question. The symbols used for the operators are explained in Fig. 3. Further, time order is from left to right. To comply with the graphical representation, we also adapt the left to right time ordering for the mathematical transcription, i.e. we write $X(\pi)\ z_3(\frac{\pi}{2})$ when $X(\pi)$ is applied first and $z_3(\frac{\pi}{2})$ second.

In this section, we present results for the three qubit code, the five qubit code and the Steane code. In a typical realization, the ground state of the ions is used to represent the qubit state $|1\rangle$. Therefore, we also use the $|1\rangle$ as initial value for all qubits, contrary to the more common $|0\rangle$ state, which we used e.g., in Figs. 1 and 2.

Readers who are interested in the details of the algorithm used to obtain the results of this section find a description in App. B.

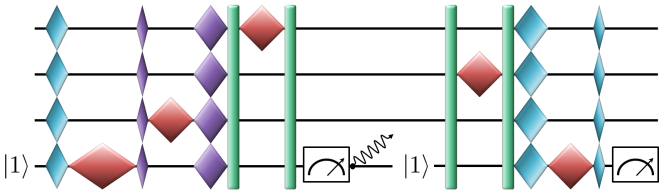

Figure 4: Measurement of the error syndrome for the three qubit bit-flip error correction code (33). The first three qubits encode the logical qubit. After the first measurement, the auxiliary qubit is reset (wavy line).

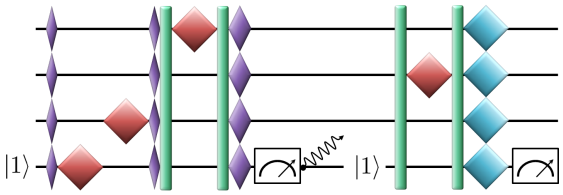

Figure 5: Measurement of the error syndrome for the three qubit phase-flip error correction code (34). The first three qubits encode the logical qubit. After the first measurement, the auxiliary qubit is reset (wavy line).

A. Three qubit code

Here, we treat the three qubit bit-flip and three qubit phase-flip error correction codes [5]. Both are realized on $3+1$ qubits, where the first three physical qubits encode the logical qubit and the fourth qubit is an auxiliary qubit initialized to the $|1\rangle$ state.

We start with the readout of the error syndrome for the bit-flip error correction code (equivalent to the quantum circuit shown in Fig. 2). Here, the codewords for the logical qubit are $|0_L\rangle = |000\rangle$, $|1_L\rangle = |111\rangle$. The following sequence maps the error syndrome onto the auxiliary qubit

$$\begin{array}{lllll} Y\left(-\frac{\pi}{2}\right) & z_4\left(-\frac{\pi}{2}\right) & X\left(-\frac{\pi}{4}\right) & z_3\left(\pi\right) & X\left(\frac{3}{4}\pi\right) \\ X^2\left(\frac{\pi}{4}\right) & z_1\left(\pi\right) & X^2\left(\frac{\pi}{4}\right) & M_4\ R_4 & X^2\left(\frac{\pi}{4}\right) \\ z_2\left(\pi\right) & X^2\left(\frac{\pi}{4}\right) & Y\left(-\frac{3}{4}\pi\right) & z_4\left(\pi\right) & Y\left(\frac{\pi}{4}\right)\ M_4. \end{array} \tag{33}$$

The graphical representation is shown in Fig. 4. For the optimization of this sequence, we actually used five qubits in the computation (two auxiliary qubits). As a direct benefit, the first measurement can be replaced by a swap gate which exchanges the first auxiliary qubit with the second. In that way, both measurements are postponed to the end of the sequence.

For trapped ions, phase errors are usually a bigger issue than bit-flip errors. Therefore, we also present an analog sequence to read out the syndrome for phase errors

$$\begin{array}{lllll} X\left(\frac{\pi}{4}\right) & z_4\left(\pi\right) & z_3\left(\pi\right) & X\left(-\frac{\pi}{4}\right) & X^2\left(\frac{\pi}{4}\right) \\ z_1\left(\pi\right) & X^2\left(\frac{\pi}{4}\right) & X\left(\frac{\pi}{2}\right) & M_4\ R_4 & X^2\left(\frac{\pi}{4}\right) \\ z_2\left(\pi\right) & X^2\left(\frac{\pi}{4}\right) & Y\left(\pi\right) & M_4, & \end{array} \tag{34}$$

where the codewords for the logical qubit are $|0_L\rangle = |+,+,+\rangle$ and $|1_L\rangle = |-,-,-\rangle$. The graphical representation is shown in Fig. 5.

Next, we look into a measurement-free coherent version of the bit-flip error correction on four qubits. Fig. 6 shows suitable sequence for this task. Although no measurement is needed in this case, the auxiliary qubit has to be reset to remove the entropy from the qubit system (first reset is mandatory, second is optional). For trapped ions, resetting a qubit can be done with much less disturbance than a measurement. But this advantage comes with a high price in the length of the sequence,

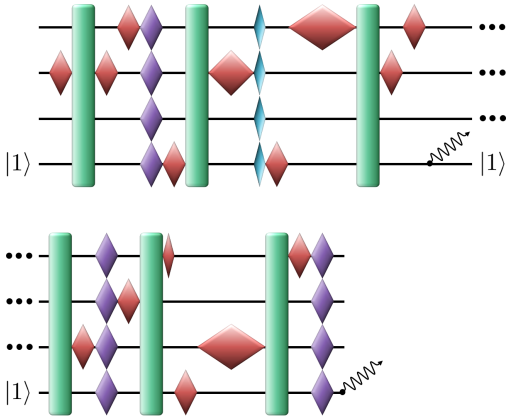

Figure 6: Coherent three qubit bit-flip error correction code (35), which corrects a possible error on the logical qubit (encoded in the first three physical qubits) without the need of a measurement. To remove the entropy, the auxiliary qubit has to be reset (wavy line). Because of its length, the sequence is split into two parts.

$$\begin{array}{lllll} z_2\left(\frac{\pi}{2}\right) & X^2\left(\frac{\pi}{2}\right) & z_2\left(\frac{\pi}{2}\right) & z_1\left(\frac{\pi}{2}\right) & X\left(\frac{\pi}{2}\right) \\ z_4\left(\frac{\pi}{2}\right) & X^2\left(\frac{\pi}{2}\right) & z_2\left(\pi\right) & Y\left(-\frac{\pi}{4}\right) & z_4\left(\frac{\pi}{2}\right) \\ z_1\left(-\frac{\pi}{2}\right) & X^2\left(\frac{\pi}{2}\right) & z_2\left(\frac{\pi}{2}\right) & z_1\left(\frac{\pi}{2}\right) & R_4 \\ X^2\left(\frac{\pi}{2}\right) & z_3\left(\frac{\pi}{2}\right) & X\left(\frac{\pi}{2}\right) & z_2\left(\frac{\pi}{2}\right) & X^2\left(\frac{\pi}{2}\right) \\ z_1\left(\frac{\pi}{4}\right) & z_4\left(\frac{\pi}{2}\right) & z_3\left(-\frac{\pi}{2}\right) & X^2\left(\frac{\pi}{2}\right) & z_1\left(\frac{\pi}{2}\right) \\ X\left(\frac{\pi}{2}\right) & R_4. & & & \end{array} \tag{35}$$

We mainly included this example to have a comparison between a measurement-based and a measurement-free QEC code. Therefore, a similar structure was adapted for both codes. For a practical realization, one might prefer the measurement-free approach whose successful experimental realization we presented in Ref. [15].

B. Five qubit code and Steane code

In this section, the five qubit code [6] and the Steane code [7] are compared. Both are stabilizer codes [2, 12] and promising candidates for future experiments, since they allow us to detect arbitrary single qubit errors. For both codes, we demonstrate how the logical qubit states

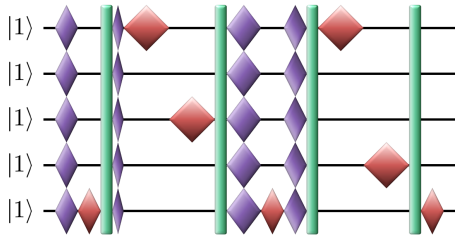

Figure 7: Sequence to generate the logical five qubit codeword $|0_L\rangle$ (37).

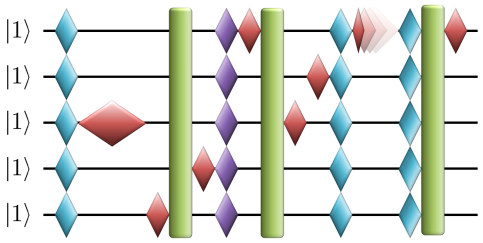

Figure 8: Sequence to generate the logical superposition state $\sin(\alpha)\cdot|0_L\rangle+\cos(\alpha)\cdot|1_L\rangle$ for the five qubit code (38). The length Θ of the second last $z_1(\Theta)$ operation depends on the angle α, i.e., $z_1(\Theta=2\alpha)$.

can be generated, how the stabilizers can be measured, and how some nontrivial logical gates might be applied.

1. *State preparation for logical qubits*

The preparation of a predefined quantum state does not allow for any variation except the global phase. Therefore, it is actually not the best example to demonstrate the ideas outlined in Secs. II and III. Still, since the preparation of logical qubit is currently a hot topic and a necessary precondition for further QEC operations, we think it is adequate to include some sequences which can be used for this purpose.

For the five qubit code, the codeword for the logical zero state [2] is

$$\begin{aligned}|0_L\rangle =&\frac{1}{4}[|00000\rangle+|10010\rangle+|01001\rangle+|10100\rangle\\&+|01010\rangle-|11011\rangle-|00110\rangle-|11000\rangle\\&-|11101\rangle-|00011\rangle-|11110\rangle-|01111\rangle\\&-|10001\rangle-|01100\rangle-|10111\rangle+|00101\rangle].\end{aligned}\quad(36)$$

The logical one state $|1_L\rangle$ is obtained from $|0_L\rangle$ by inverting all qubits ($0\leftrightarrow1$).

Starting with the product state $|11111\rangle$, the logical zero state $|0_L\rangle$ can be generated applying the following sequence (Fig. 7):

$$\begin{array}{lllll}X\left(\frac{\pi}{2}\right) & z_5\left(\frac{\pi}{2}\right) & X^2\left(\frac{\pi}{4}\right) & X\left(-\frac{\pi}{4}\right) & z_1(\pi)\\ z_3(\pi) & X^2\left(\frac{\pi}{4}\right) & X\left(\frac{3}{4}\pi\right) & z_5\left(\frac{\pi}{2}\right) & X\left(-\frac{\pi}{2}\right)\\ X^2\left(\frac{\pi}{4}\right) & z_1(\pi) & z_4(\pi) & X^2\left(\frac{\pi}{4}\right) & z_5\left(\frac{\pi}{2}\right)\end{array}\quad(37)$$

Replacing the first three $X(\Theta)$ and the last $z_5\left(\frac{\pi}{2}\right)$ in this sequence by their inverse operations results in the logical one state $|1_L\rangle$.

Alternatively, one can use the following sequence (Fig. 8) to obtain the logical superposition state $\sin(\alpha)\cdot|0_L\rangle+\cos(\alpha)\cdot|1_L\rangle$, with arbitrary but known α,

$$\begin{array}{llll}Y\left(\frac{\pi}{2}\right) & z_3\left(-\frac{\pi}{2}\right) & z_5\left(\frac{\pi}{2}\right) & Y^2\left(\frac{\pi}{2}\right) & z_4\left(\frac{\pi}{2}\right)\\ X\left(\frac{\pi}{2}\right) & z_1\left(\frac{\pi}{2}\right) & Y^2\left(\frac{\pi}{2}\right) & z_3\left(\frac{\pi}{2}\right) & z_2\left(\frac{\pi}{2}\right)\\ Y\left(\frac{\pi}{2}\right) & z_1(2\alpha) & Y\left(-\frac{\pi}{2}\right) & Y^2\left(\frac{\pi}{2}\right) & z_1\left(\frac{\pi}{2}\right)\end{array}\quad(38)$$

If the first $Y\left(\frac{\pi}{2}\right)$ is replaced by $Y\left(-\frac{\pi}{2}\right)$ the result of the sequence is $\cos(\alpha)\cdot|0_L\rangle-\sin(\alpha)\cdot|1_L\rangle$. This replacement is e.g. of interest to produce the zero state $|0_L\rangle$, which can now be done by setting $\alpha=0$. This allows us to omit the subsequence $Y\left(\frac{\pi}{2}\right)\ z_1(2\alpha=0)\ Y\left(-\frac{\pi}{2}\right)$, resulting in the shortest sequence found for $|0_L\rangle$.

The reader might wonder how the optimization for such a sequence with an open parameter α was done. The trick is that such sequences can be found using a *fixed* α. To see this, we first note that the optimal sequences which generate the states $|0_L\rangle$ respectively $|1_L\rangle$ are all built up by operations with quantized arguments $\Theta_j=\frac{m_j}{2^{n_j}}\cdot\pi$, with $m_j\in\mathbb{Z}$, $n_j\in\mathbb{N}_0$. But if we choose to generate the state $\sin(\alpha)\cdot|0_L\rangle+\cos(\alpha)\cdot|1_L\rangle$ with a fixed angle α that does not fit into this quantization scheme (e.g., $\alpha=\frac{\pi}{5}$), at least one operation is needed with an argument $\Theta_k\neq\frac{m}{2^n}\cdot\pi$. Looking into various different sequences that contain exactly one such operation with an argument $\Theta_k\neq\frac{m}{2^n}\cdot\pi$, we found that for some of these sequences the argument $\Theta_k=\Theta_k(\alpha)$ could be expressed as a (linear) function of α. In other words, some sequences, which were found for a specific value of α, can be generalized to arbitrary values of α by adopting the argument $\Theta_k(\alpha)$, while all other arguments $\Theta_{j\neq k}$ stay unchanged, as in Eq. (38) with its $z_1(\Theta=2\alpha)$ operation.

If we try to introduce a further phase factor $\sin(\alpha)\cdot|0_L\rangle+e^{i\beta}\cos(\alpha)\cdot|1_L\rangle$ we need at least two operations with arguments $\Theta_k\neq\frac{m}{2^n}\cdot\pi$. We found several of such sequences which are generalizable to arbitrary α and β, but the values of the two corresponding arguments $\Theta_k(\alpha,\beta)$ have to be determined numerically. None of them shows a simple linear relation $\Theta_k(\alpha,\beta)\propto\alpha,\beta$ nor any other evident analytical dependence on the chosen angles α,β, which would allow us to present these results.

For the Steane code, the codeword for the logical zero state [2] is

$$\begin{aligned}|0_L\rangle =&\frac{1}{\sqrt{8}}\big[|0000000\rangle+|1010101\rangle+|0110011\rangle\\&+|1100110\rangle+|0001111\rangle+|1011010\rangle\\&+|0111100\rangle+|1101001\rangle\big]\end{aligned}\quad(39)$$

and the logical one state $|1_L\rangle$ can be obtained from $|0_L\rangle$ by inverting all qubits ($0\leftrightarrow1$). Analog to the five qubit code, we can list a sequence (Fig. 9) to produce the logical

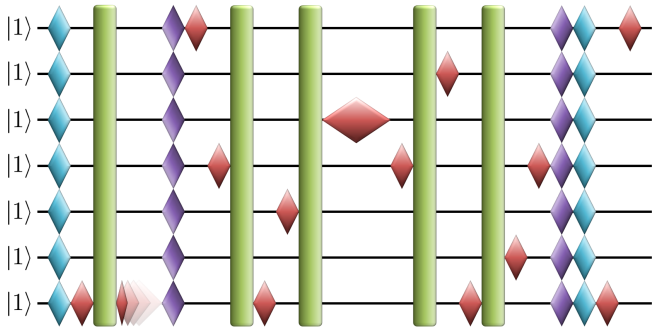

Figure 9: Sequence to generate the logical superposition state $\cos(\alpha)\cdot|0_L\rangle+\sin(\alpha)\cdot|1_L\rangle$ for the Steane code (40). The length Θ of the second $z_7(\Theta)$ operation depends on the angle α, i.e., $z_7(\Theta = 2\alpha - \frac{\pi}{2})$.

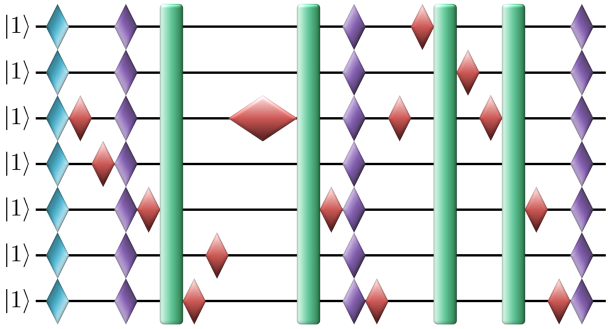

Figure 10: Sequence to generate the logical Steane codeword $|0_L\rangle$ (41).

superposition state $\cos(\alpha)\cdot|0_L\rangle+\sin(\alpha)\cdot|1_L\rangle$ out of the product state $|1111111\rangle$,

$$\begin{array}{lllll} Y\left(\frac{\pi}{2}\right) & z_7\left(\frac{\pi}{2}\right) & Y^2\left(\frac{\pi}{2}\right) & z_7\left(2\alpha-\frac{\pi}{2}\right) & X\left(-\frac{\pi}{2}\right) \\ z_1\left(\frac{\pi}{2}\right) & z_4\left(\frac{\pi}{2}\right) & Y^2\left(\frac{\pi}{2}\right) & z_7\left(\frac{\pi}{2}\right) & z_5\left(\frac{\pi}{2}\right) \\ Y^2\left(\frac{\pi}{2}\right) & z_3\left(-\frac{\pi}{2}\right) & z_4\left(\frac{\pi}{2}\right) & Y^2\left(\frac{\pi}{2}\right) & z_2\left(\frac{\pi}{2}\right) \\ z_7\left(\frac{\pi}{2}\right) & Y^2\left(\frac{\pi}{2}\right) & z_6\left(\frac{\pi}{2}\right) & z_4\left(\frac{\pi}{2}\right) & X\left(\frac{\pi}{2}\right) \\ Y\left(\frac{\pi}{2}\right) & z_7\left(\frac{\pi}{2}\right) & z_1\left(\frac{\pi}{2}\right). & & \end{array} \tag{40}$$

Contrary to the five qubit code, where the shortest sequences for $|0_L\rangle$ and $|1_L\rangle$ could be found by setting $\alpha = 0$ in Eq. (38), for the Steane code it is better to resort to alternative sequences for the logical codewords $|0_L\rangle$ and $|1_L\rangle$. We found sequences consisting of only 19 operations, but with five Mølmer-Sørensen (MS) gates ($X^2\left(\frac{\pi}{2}\right)$ or $Y^2\left(\frac{\pi}{2}\right)$), as above (40). Since the MS gates are the main source for losses in fidelity, another sequence to create the logical zero state $|0_L\rangle$ with 22 operations but only four MS gates might be more favorable (Fig. 10),

$$\begin{array}{lllll} Y\left(-\frac{\pi}{2}\right) & z_3\left(\frac{\pi}{2}\right) & z_4\left(\frac{\pi}{2}\right) & X\left(-\frac{\pi}{2}\right) & z_5\left(\frac{\pi}{2}\right) \\ X^2\left(\frac{\pi}{2}\right) & z_7\left(\frac{\pi}{2}\right) & z_6\left(\frac{\pi}{2}\right) & z_3\left(-\frac{\pi}{2}\right) & X^2\left(\frac{\pi}{2}\right) \\ z_5\left(\frac{\pi}{2}\right) & X\left(\frac{\pi}{2}\right) & z_7\left(\frac{\pi}{2}\right) & z_3\left(\frac{\pi}{2}\right) & z_1\left(\frac{\pi}{2}\right) \\ X^2\left(\frac{\pi}{2}\right) & z_2\left(\frac{\pi}{2}\right) & z_3\left(\frac{\pi}{2}\right) & X^2\left(\frac{\pi}{2}\right) & z_5\left(\frac{\pi}{2}\right) \\ z_7\left(\frac{\pi}{2}\right) & X\left(-\frac{\pi}{2}\right). & & & \end{array} \tag{41}$$

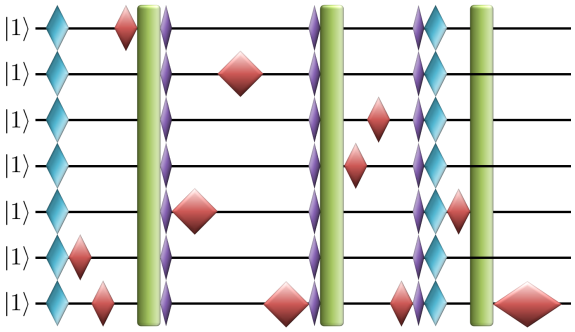

Figure 11: Sequence to generate the logical Steane codeword $|0_L\rangle$ (42). The third Mølmer-Sørensen gate only acts on the qubits number 1, 3, 5, and 7.

Replacing the first operator $Y\left(-\frac{\pi}{2}\right)$ by its inverse $Y\left(\frac{\pi}{2}\right)$ allows us to generate the logical one state $|1_L\rangle$.

In Ref. [16], a logical state (color-code) is created with the help of MS gates which operate solely on subsets of the entire seven qubits. Inspired by this work, we present a further alternative to create the $|0_L\rangle$ state. Here, we come along with three MS gates $Y^2\left(\frac{\pi}{2}\right)$, where the last (third) MS gate $\tilde{Y}^2_{1,3,5,7}\left(\frac{\pi}{2}\right)$ operates only on the qubits number 1, 3, 5, and 7 (Fig. 11),

$$\begin{array}{llll} Y\left(-\frac{\pi}{2}\right) & z_6\left(\frac{\pi}{2}\right) & z_7\left(\frac{\pi}{2}\right) & z_1\left(\frac{\pi}{2}\right) \quad Y^2\left(\frac{\pi}{2}\right) \\ X\left(\frac{\pi}{4}\right) & z_5\left(\pi\right) & z_2\left(\pi\right) & z_7\left(\pi\right) \quad X\left(\frac{\pi}{4}\right) \\ Y^2\left(\frac{\pi}{2}\right) & z_4\left(\frac{\pi}{2}\right) & z_3\left(\frac{\pi}{2}\right) & z_7\left(\frac{\pi}{2}\right) \quad X\left(\frac{\pi}{4}\right) \\ Y\left(-\frac{\pi}{2}\right) & z_5\left(\frac{\pi}{2}\right) & \tilde{Y}^2_{1,3,5,7}\left(\frac{\pi}{2}\right) & z_7\left(-\frac{\pi}{2}\right). \end{array} \tag{42}$$

Some more comments concerning MS gates on subsets can be found in App. A.

2. *Stabilizer*

The five qubit code and the Steane code are examples for stabilizer codes. A stabilizer is a product of local Pauli operators and the identity, e.g., the first (of four) stabilizer of the five qubit code is given by $XZZXI$ (which is shorthand for $\sigma_x^{(1)}\cdot\sigma_z^{(2)}\cdot\sigma_z^{(3)}\cdot\sigma_x^{(4)}\cdot\mathbb{1}^{(5)}$); see Tab. I. The measurement result of the stabilizers does not reveal the state of the logical qubit, but it allows us to infer which error might have happened. To measure a stabilizer, its result is mapped onto an auxiliary qubit, which then can be read out. In short: the situation complies with the measurement of the syndrome discussed in Sec. II A 1.

For the five qubit code, the four stabilizers (Tab. I) are related by cyclical permutation. Therefore, it suffices to list the sequence (Fig. 12) of the first stabilizer ($XZZXI$) – the others follow by cyclical permutation of the local $z_j(\Theta)$ operators in the sequence (not including the operator $z_6(\pi)$ acting on the auxiliary qubit!)

$$\begin{array}{lllll} X\left(-\frac{\pi}{2}\right) & z_2\left(\frac{\pi}{2}\right) & z_3\left(\frac{\pi}{2}\right) & X\left(\frac{\pi}{4}\right) & X^2\left(\frac{\pi}{4}\right) \\ z_5\left(\pi\right) & X^2\left(\frac{\pi}{4}\right) & z_6\left(\pi\right) & X\left(\frac{\pi}{4}\right) & z_2\left(\frac{\pi}{2}\right) \\ z_3\left(\frac{\pi}{2}\right) & X\left(-\frac{\pi}{2}\right) & z_5\left(\pi\right) & M_6. & \end{array} \tag{43}$$

Number	Operator
1	$XZZXI$
2	$IXZZX$
3	$XIXZZ$
4	$ZXIXZ$

Table I: Description of the four stabilizers for the five qubit code.

Number	Operator
1	$IIIXXXX$
2	$IXXIIXX$
3	$XIXIXIX$
4	$IIIZZZZ$
5	$IZZIIZZ$
6	$ZIZIZIZ$

Table II: Description of the six stabilizers for the Steane code.

To detect an error, all four stabilizers have to be measured. Instead of applying all four stabilizer sequences individually, one might also use the following sequence to get the four results (Fig. 13):

$$\begin{array}{lllll} z_3\left(\frac{\pi}{2}\right) & X\left(\frac{\pi}{2}\right) & z_3\left(\frac{\pi}{2}\right) & z_2\left(\frac{\pi}{2}\right) & X^2\left(\frac{\pi}{4}\right) \\ z_5\left(\pi\right) & X^2\left(\frac{\pi}{4}\right) & z_2\left(\frac{\pi}{2}\right) & X\left(-\frac{\pi}{2}\right) & z_2\left(\frac{\pi}{2}\right) \\ z_4\left(\frac{\pi}{2}\right) & M_6\ R_6 & X^2\left(\frac{\pi}{4}\right) & z_1\left(\pi\right) & X^2\left(\frac{\pi}{4}\right) \\ z_3\left(\frac{\pi}{2}\right) & M_6\ R_6 & z_5\left(\frac{\pi}{2}\right) & X^2\left(\frac{\pi}{4}\right) & z_2\left(\pi\right) \\ X^2\left(\frac{\pi}{4}\right) & z_4\left(\frac{\pi}{2}\right) & z_1\left(\frac{\pi}{2}\right) & M_6\ R_6 & X\left(-\frac{\pi}{2}\right) \\ z_1\left(\frac{\pi}{2}\right) & X^2\left(\frac{\pi}{4}\right) & z_3\left(\pi\right) & X^2\left(\frac{\pi}{4}\right) & z_1\left(\frac{\pi}{2}\right) \\ z_5\left(\frac{\pi}{2}\right) & X\left(\frac{\pi}{2}\right) & z_5\left(\frac{\pi}{2}\right) & M_6. & \end{array} \tag{44}$$

Here, we actually used nine qubits for the optimization and replaced the first three measurements by swap gates to avoid measurements within the sequence. This is basically the same trick as described for Eq. (33).

The sequence we found consists of only 30 unitary operations, which has to be compared with $4 \times 13 = 52$ for the sum of the unitary operations of all four individual stabilizers. The ratio of the needed operations becomes

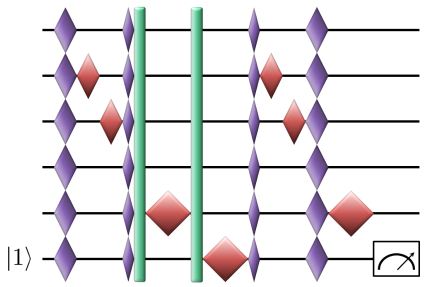

Figure 12: Measurement of the stabilizer ($XZZXI$) for the five qubit code (43).

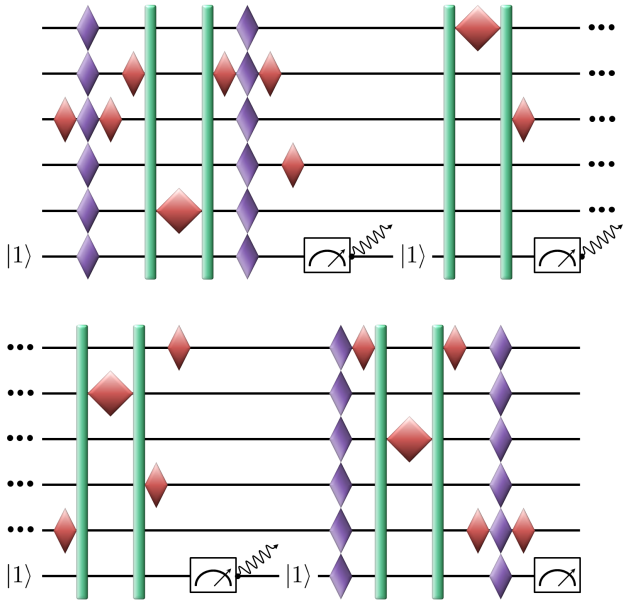

Figure 13: Measurement of all four stabilizers for the five qubit code (44). Because of its length, the sequence is split into two parts. After the first three measurements, the auxiliary qubit is reset.

even more impressive when we take into account that the number of the Mølmer-Sørensen (MS) gates $X^2(\frac{\pi}{4})$ could not be altered. To entangle two formerly unentangled qubits, one needs at least two $X^2(\frac{\pi}{4})$ gates. Since the auxiliary qubit has to be entangled four times with the code qubits, the minimal number of $X^2(\frac{\pi}{4})$ gates is eight. With that in mind, the comparison to be made is $30 - 8 = 22$ versus $52 - 8 = 44$, which is a factor of two!

Contrary to all other sequences presented in this paper, this is the only one which is not the result of an ab initio calculation starting from a random sequence. The start sequence was a composite of previous results for the single stabilizers, which were optimized with the help of the method described in App. B 3 a.

With an increasing complexity of future quantum algorithms we might face much more tasks which can only be solved with the help of composite sequences. Therefore, it seems very promising that we managed to reduce the number of the non Mølmer-Sørensen gates by a factor of two. Unfortunately, a great part of the savings might only be due to the gauge freedom and the fact that the four stabilizers are realized by quite similar quantum circuits. If this is the case, the four-stabilizer-sequence is just a positive exception. Anyway, it still seems a realistic hope that similar savings could be achievable when the four stabilizers are optimized for other quantum systems.

For the Steane code, the sequences for all six stabilizers (Tab. II) can be derived from two base sequences. To measure the first stabilizer ($IIIXXXX$), one can use

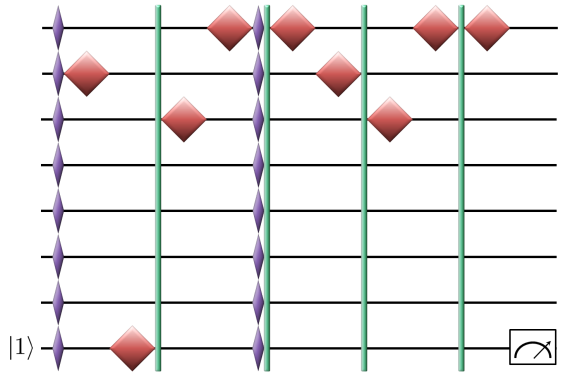

Figure 14: Measurement of the first stabilizer ($IIIXXXX$) for the Steane code (45).

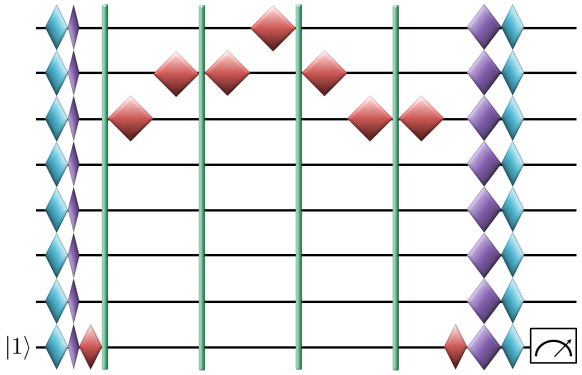

Figure 15: Measurement of the fourth stabilizer ($IIIZZZZ$) for the Steane code (47).

the sequence (Fig. 14):

$$\begin{array}{ccccc} X\left(\frac{\pi}{4}\right) & z_2(\pi) & z_8(\pi) & X^2\left(\frac{\pi}{8}\right) & z_3(\pi) \\ z_1(\pi) & X\left(\frac{\pi}{4}\right) & X^2\left(\frac{\pi}{8}\right) & z_1(\pi) & z_2(\pi) \\ X^2\left(\frac{\pi}{8}\right) & z_3(\pi) & z_1(\pi) & X^2\left(\frac{\pi}{8}\right) & z_1(\pi)\ M_8. \end{array} \tag{45}$$

Observe that the local $z_j(\pi)$ operators act only on positions where the stabilizer has an identity I (and on the auxiliary qubit). To get the second and the third stabilizer (see Tab. II), the only thing to do is to rearrange the $z_j(\pi)$ accordingly to the identities in these stabilizers

$$\begin{aligned} \underbrace{(z_1(\pi); z_2(\pi); z_3(\pi))}_{\text{first stabilizer}} &\rightarrow \underbrace{(z_1(\pi); z_4(\pi); z_5(\pi))}_{\text{second stabilizer}} \\ &\rightarrow \underbrace{(z_2(\pi); z_4(\pi); z_6(\pi))}_{\text{third stabilizer}}. \end{aligned} \tag{46}$$

This rearrangement might not be trivial, but still, it works. Moreover, the same rearrangement trick of the $z_j(\pi)$ can also be applied to derive the sequences for the fifth and sixth stabilizer from the sequence of the fourth stabilizer, which is given by (Fig. 15)

$$\begin{array}{ccccc} Y\left(\frac{\pi}{2}\right) & X\left(-\frac{\pi}{4}\right) & z_8\left(\frac{\pi}{2}\right) & X^2\left(\frac{\pi}{8}\right) & z_3(\pi) \\ z_2(\pi) & X^2\left(\frac{\pi}{8}\right) & z_2(\pi) & z_1(\pi) & X^2\left(\frac{\pi}{8}\right) \\ z_2(\pi) & z_3(\pi) & X^2\left(\frac{\pi}{8}\right) & z_3(\pi) & z_8\left(\frac{\pi}{2}\right) \\ X\left(\frac{3}{4}\pi\right) & Y\left(\frac{\pi}{2}\right) & M_8. & & \end{array} \tag{47}$$

It goes without saying that alternative sequences can be found, as well. Here, we presented solutions for the five qubit code and the Steane code which contain the minimal total length $\sum_{X^2}|\Theta|$ of Mølmer-Sørensen (MS) gates $X^2(\Theta)$ needed to entangle the formerly unentangled auxiliary qubit with the code qubits: The Steane code needs four $X^2\left(\Theta=\frac{\pi}{8}\right)$ gates and the five qubit code two $X^2\left(\Theta=\frac{\pi}{4}\right)$ gates, which in both cases sums up to the minimal value $\sum_{X^2}|\Theta|=\frac{\pi}{2}$. For $\sum_{X^2}|\Theta|<\frac{\pi}{2}$, only partial entanglement can be achieved, while $\sum_{X^2}|\Theta|>\frac{\pi}{2}$ is possible as well.

For a practical realization on the other hand, other aspects than the length $\sum_{X^2}|\Theta|$ might become more important. In experiments, one might want to apply a stabilizer sequence after a state preparation sequence. The state preparation sequences for the Steane code (40) (41) are built on $Y^2(\frac{\pi}{2})$ and $X^2(\frac{\pi}{2})$ gates, while the stabilizer sequence uses $X^2\left(\frac{\pi}{8}\right)$ gates. As long as it is experimentally advisable to use just one type of MS gate, these two sequences are not a perfect match. Under this condition, it seems favorable to resort to other sequences, which might appear suboptimal when treated as isolated. Alternatively, one could also consider to replace each $X^2\left(\frac{\pi}{2}\right)$ by four consecutive $X^2\left(\frac{\pi}{8}\right)$. Usually, such a replacement also entails a certain loss in the experimental fidelity.

3. *Logical gates*

Depending on the QEC code, some logical gates are transversal. That is, they can be implemented in a bitwise fashion [2], i.e., by mere local operations in the case of logical gates which act only on a single logical qubit. In the five qubit code, the logical σ_x, σ_y, and σ_z operations are of such kind, while the logical Hadamard gate $\frac{1}{\sqrt{2}}\begin{pmatrix}1 & 1\\ 1 & -1\end{pmatrix}$ is not. In the Steane code on the other hand, the logical Hadamard gate and even the logical CNOT gate are transversal, as well (next to the logical σ_x, σ_y, and σ_z operations) [2]. Unfortunately, neither the logical $\frac{\pi}{8}$ gate $\begin{pmatrix}1 & 1\\ 1 & e^{i\frac{\pi}{4}}\end{pmatrix}$ is transversal nor any other gate which could complement the transversal gates of the Steane code to a universal set of logical gates.

Therefore, we have chosen the logical Hadamard gate for the five qubit code and the logical $\frac{\pi}{8}$ gate for the Steane code as non trivial examples for logical gates. The presented sequences do not amplify any correctable error present on the logical qubit (Sec. II C). Abandoning this

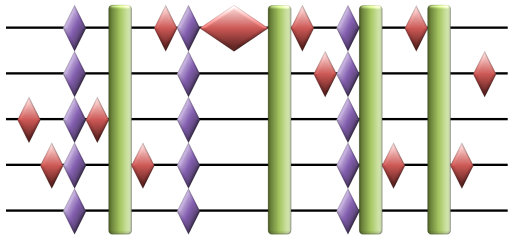

Figure 16: Logical Hadamard gate for the five qubit code (48).

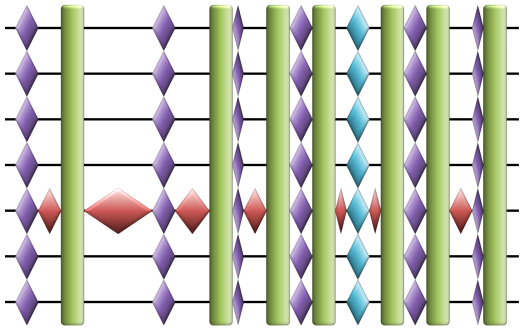

Figure 17: Logical $\frac{\pi}{8}$ gate for the Steane code (49).

property would result in much simpler sequences for the logical gates.

For the five qubit code, the logical Hadamard gate $\frac{1}{\sqrt{2}}\begin{pmatrix} 1 & 1 \\ 1 & -1 \end{pmatrix}$ (Fig. 16) can be implemented by the following sequence:

$$\begin{array}{llll} z_3\left(\frac{\pi}{2}\right) & z_4\left(\frac{\pi}{2}\right) & X\left(\frac{\pi}{2}\right) & z_3\left(\frac{\pi}{2}\right) \quad Y^2\left(\frac{\pi}{2}\right) \\ z_4\left(\frac{\pi}{2}\right) & z_1\left(\frac{\pi}{2}\right) & X\left(\frac{\pi}{2}\right) & z_1\left(-\frac{\pi}{2}\right) \quad Y^2\left(\frac{\pi}{2}\right) \\ z_1\left(\frac{\pi}{2}\right) & z_2\left(\frac{\pi}{2}\right) & X\left(\frac{\pi}{2}\right) & Y^2\left(\frac{\pi}{2}\right) \quad z_4\left(\frac{\pi}{2}\right) \\ z_1\left(\frac{\pi}{2}\right) & Y^2\left(\frac{\pi}{2}\right) & z_4\left(\frac{\pi}{2}\right) & z_2\left(\frac{\pi}{2}\right). \end{array} \tag{48}$$

For the Steane code, the logical $\frac{\pi}{8}$ gate $\begin{pmatrix} 1 & 1 \\ 1 & e^{i\frac{\pi}{4}} \end{pmatrix}$ (Fig. 17) can be realized via

$$\begin{array}{lllll} X\left(\frac{\pi}{2}\right) & z_5\left(\frac{\pi}{2}\right) & Y^2\left(\frac{\pi}{2}\right) & z_5\left(-\frac{\pi}{2}\right) & X\left(\frac{\pi}{2}\right) \\ z_5\left(\frac{3}{4}\pi\right) & Y^2\left(\frac{\pi}{2}\right) & X\left(-\frac{\pi}{4}\right) & z_5\left(\frac{\pi}{2}\right) & Y^2\left(\frac{\pi}{2}\right) \\ X\left(\frac{\pi}{2}\right) & Y^2\left(\frac{\pi}{2}\right) & z_5\left(\frac{\pi}{4}\right) & Y\left(\frac{\pi}{2}\right) & z_5\left(\frac{\pi}{4}\right) \\ Y^2\left(\frac{\pi}{2}\right) & X\left(\frac{\pi}{2}\right) & Y^2\left(\frac{\pi}{2}\right) & z_5\left(\frac{\pi}{2}\right) & X\left(-\frac{\pi}{4}\right) \\ Y^2\left(\frac{\pi}{2}\right). & & & & \end{array} \tag{49}$$

We remark that we also searched for sequences with an open parameter α for arbitrary logical rotations $U_L(\alpha)$ of the type

$$U_L(\alpha) = \begin{pmatrix} 1 & 1 \\ 1 & e^{i\alpha} \end{pmatrix}. \tag{50}$$

For the five qubit code, this search had to be terminated unsuccessful, but for the Steane code, we managed to find such sequences for variable $U_L(\alpha)$. While the sequences for the state preparation with an open parameter α contain just one operation with an adjustable argument (38) and (40), the best sequences found for $U_L(\alpha)$ come with four such operations. Of these four operations, only one shows a linear correspondence between its argument and the parameter α. For the other three, we were not able to determine an analytical relation, which would have allowed us to communicate these findings as a reproducible formula.

V. CONCLUSION

In conclusion, we have studied the gauge freedoms inherent in quantum algorithms used for quantum error correction codes as well as in logical operations on qubits in error protected states. We showed how these gauge freedoms translate into specially chosen performance functions suitable for optimal control algorithms. This allowed us to improve the decomposition of the corresponding quantum algorithms into sequences of elementary operations. These general ideas are complemented by an in-detail description of an example algorithm tailored for experiments with trapped ions (App. B). As a result, various decompositions were presented, comprising quantum algorithms for the three qubit, the five qubit, and the Steane code. All these decompositions are exact and allow intuitive representation as quantum circuits. The unitaries used for the decompositions can all be implemented with fairly high fidelities on trapped ions such that one might be optimistic to see experiments which realize some of the more advanced quantum error correction codes in the near future.

VI. ACKNOWLEDGMENTS

This research was funded by the Austrian Science Fund (FWF): P24273-N16, SFB F40-FoQus F4012-N16 and by the Austrian Ministry of Science BMWF as part of the UniInfrastrukturprogramm of the Research Platform Scientific Computing at the University of Innsbruck. I like to thank the group of Prof. Rainer Blatt for their cooperation and the insights into the experimental aspects of quantum computation, with special thanks (in alphabetic order) to Thomas Monz, Daniel Nigg, Christian Roos and Philipp Schindler. Further, I like to thank my supervisor Wolfgang Dür for the freedom to pursue my own ideas.

I'm currently looking for a PostDoc position.

[1] A. Barenco, C. H. Bennett, R. Cleve, D. P. DiVincenzo, N. Margolus, P. Shor, T. Sleator, J. A. Smolin, and H. Weinfurter, *Phys.Rev. A*, **52**, 3457 (1995). Elementary gates for quantum computation.

[2] M. A. Nielsen and I. L. Chuang, *Quantum Computation and Quantum Information*, Cambridge Univ. Press, 2000.

[3] C. Brif, R. Chakrabarti, and H. Rabitz, *New J. Phys.*, **12**, 075008 (2010). Control of quantum phenomena: Past, present, and future.

[4] P. Schindler, D. Nigg, T. Monz, J. T. Barreiro, E. Martinez, S. X. Wang, S. Quint, M. F. Brandl, V. Nebendahl, and C. F. Roos, *New J. Phys.*, **15**, 123012 (2013). A quantum information processor with trapped ions.

[5] P. W. Shor, *Phys. Rev. A*, **52**, R2493 (1995). Scheme for reducing decoherence in quantum computer memory.

[6] R. Laflamme, C. Miquel, J. P. Paz, and W. H. Zurek, *Phys. Rev. Lett.*, **77**, 198 (1996). Perfect quantum error correcting code.

[7] A. M. Steane, *Phys. Rev. Lett.*, **77**, 793 (1996). Error correcting codes in quantum theory.

[8] D. P. DiVincenzo and P. W. Shor, *Phys. Rev. Lett*, **77**, 3260 (1996). Fault-tolerant error correction with efficient quantum codes.

[9] J. Preskill, *Proc.Roy.Soc.Lond. A*, **454**, 385–410 (1998). Reliable quantum computers.

[10] N. Khaneja, T. Reiss, C. Kehlet, T. Schulte-Herbrüggen, and S. J. Glaser, *J. Magn. Reson.*, **172**, 296 (2005). Optimal control of coupled spin dynamics: design of nmr pulse sequences by gradient ascent algorithms.

[11] S. Machnes, U. Sander, S. J. Glaser, P. de Fouquières, A. Gruslys, S. Schirmer, and T. Schulte-Herbrüggen, *Phys. Rev. A*, **84**, 022305 (2011). Comparing, optimizing, and benchmarking quantum-control algorithms in a unifying programming framework.

[12] D. Gottesman, *Phys. Rev. A*, **54**, 1862 (1996). A class of quantum error-correcting codes saturating the quantum hamming bound.

[13] K. Mølmer and A. Sørensen, *Phys. Rev. Lett.*, **82**, 1835 (1999). Multiparticle entanglement of hot trapped ions.

[14] J. Benhelm, G. Kirchmair, C. F. Roos, and R. Blatt, *Nat. Phys.*, **4**, 463 (2008). Towards fault-tolerant quantum computing with trapped ions.

[15] P. Schindler, J. T. Barreiro, T. Monz, V. Nebendahl, D. Nigg, M. Chwalla, M. Hennrich, and R. Blatt, *Science*, **332**, 1059 (2011). Experimental repetitive quantum error correction.

[16] D. Nigg, M. Müller, E. A. Martinez, P. Schindler, M. Hennrich, T. Monz, M. A. Martin-Delgado, and R. Blatt, *Science*, **345**, 302 (2014). Quantum computations on a topologically encoded qubit.

[17] J. I. Cirac and P. Zoller, *Phys. Rev. Lett*, **74**, 4091 (1995). Quantum computations with cold trapped ions.

[18] C. F. Roos, *New J. Phys.*, **10**, 013002 (2008). Ion trap quantum gates with amplitude-modulated laser beams.

[19] V. Nebendahl, H. Häffner, and C. F. Roos, *Phys. Rev. A*, **79**, 012312 (2009). Optimal control of entangling operations for trapped ion quantum computing.

[20] S. Kirkpatrick, C. D. G. Jr., and M. P. Vecchi, *Science*, **220**, 4598 (1983). Optimization by simulated annealing.

[21] More complex codes might also be able to handle two incorrect qubits, but this still counts as one error in the sense that we have to define an elementary error E_j which corresponds to the combination of two corrupted qubits. Hence, it is still just one phase factor that remains.

Appendix A: Elementary operations for trapped ions

In this section, we provide a short explanation for the choice of the effective unitaries $u_t(\alpha_t)$ made in Eq. 30. We start with the Mølmer-Sørensen (MS) gates $\exp(-i \cdot \alpha_t \cdot S_{x/y}^2)$, which were chosen because they are currently the entangling gates with the highest fidelities [14]. They entangle each ion with each other ion in the trap. A strong point of the MS gate is that up to second order in perturbation theory it is independent of the motional mode of the ions, while, e.g., the formerly used Ciarc-Zoller CNOT gate [17] explicitly relies on the assumption that the ions are in a well defined motional mode. More details can be found in Ref. [18].

For the MS gates, a bichromatic laser field is needed. Restricting to a single frequency instead of the bichromatic field, the same laser beams can be used for the collective rotations $\exp(-i \cdot \alpha_t \cdot S_{x/y})$. Further, we need some local operations to "individualize" the qubits. In the setup we have in mind, this requires an extra laser beam which can be focused on single ions only. If this requirement is not fulfilled with 100% accuracy, the neighboring ions are affected by the laser beam, as well. One advantage of the chosen single qubit phase-shift gate $\exp(-i \cdot \alpha_t \cdot \sigma_z^{(j)})$ is that it can be obtained from an ac Stark shift induced by an off-resonant laser beam. The phase shift is proportional to the intensity of the laser field and hence proportional to the square of the field amplitude. Therefore, the residual effects that the laser beam exerts on the neighboring ions drop off much faster than for operations which are only linear in the field amplitude, as would be the case for $\exp(-i \cdot \alpha_t \cdot \sigma_{x/y}^{(j)})$. As a further experimental advantage, the phase of the off-resonant laser field does not need to be synchronized with the field used for the MS gates $\exp(-i \cdot \alpha_t \cdot S_{x/y}^2)$ and the collective rotation $\exp(-i \cdot \alpha_t \cdot S_{x/y})$.

Another interesting option is to decouple ions [4], i.e., to transfer them into a state which is not affected by the laser beams used for the gate operations. Although this might simplify some operations, as, e.g., in Eq. (42), decoupling ions entails some numerical drawbacks in the context of an optimization algorithm. Either we have to increase the local Hilbert spaces from dimension two to four to accommodate the decoupled states, or we define, e.g., extra MS gates which act only on a restricted number of ions. In this case, due to the high number of combinatorial possibilities to decouple different ions, the number of elementary operations would strongly increase and most likely suffocate the optimization. This argument is of course only true for a kind of black box

optimization with no physical insight, where all possible combinations of decoupled ions are considered equally likely. If the structure of the problem at hand clearly singles out a limited amount of useful MS gates which only operate on a subset of all ions, it might be beneficial to enlarge the set of elementary operations by these gates; see, e.g., Ref. [16]. This is also true for Eq. (42), where an extra MS gate operating on a special subset was included by hand.

Appendix B: Optimization algorithm for trapped ions

In this section, we provide an in-detail description of the optimization algorithm used for finding the results presented in Sec. IV.

1. Extra criteria

So far, the only optimization objective discussed in Sec. III is to maximize the performance function $\Phi(\boldsymbol{\alpha})$, which ensures that the ansatz $\prod_t u_t(\alpha_t)$ (8) mimics the desired target operation U_{target} as well as possible. For trapped ions, further criteria are of importance. Due to the reduction to effective unitary operations, perfect solutions are found much more frequently, which brings with it the need to define a ranking of these otherwise perfect solutions.

a. First criterion

As primary criterion, we demand that the optimal sequence of the effective unitary operations $\prod_{t=0}^{T} u_t(\alpha_t)$ be short in number (small T). That is, we have a few $u_t(\alpha_t)$ with big values of α_t rather than a lot of $u_t(\alpha_t)$ with small values of α_t. Under this conditions, it might seem that the arguments α_t are not the only unknown components in the optimization problem, since we are neither a priori aware of the minimal number of unitaries needed, nor do we know the order of the different effective Hamiltonians H_j we have to apply.

The solution we adopt to find a short sequence of correctly ordered unitaries is to start with a large (random) sequence $\prod u_t(\alpha_t^{\text{inital}})$ and gradually remove dispensable unitaries during the optimization process. To gradually remove these unitaries, it suffices to include side conditions which force most of the α_t to turn stepwise into zero. These side conditions have to be adjusted individually for each α_t such that they exert strong pressure on the majority of unimportant $u_t(\alpha_t)$, while the few important $u_t(\alpha_t)$ only be influenced marginally. Of course, we can only judge the importance of a given unitary $u_k(\alpha_k)$ at the actual moment in the optimization, which might differ from its final importance at the end of the optimization.

In Ref. [19], we derived the importance from the length of α_k. Here, we use an alternative method and define the importance I of a unitary $u_k(\alpha_k)$ as the difference

$$I\left[u_k(\alpha_k)\right] = \Phi(\boldsymbol{\alpha}) - \Phi^{\bar{k}}(\boldsymbol{\alpha}), \tag{B1}$$

where $\Phi(\boldsymbol{\alpha})$ is the regular performance function obtained from the actual sequence $\prod_{t=0}^{T} u_t(\alpha_t)$, while $\Phi^{\bar{k}}(\boldsymbol{\alpha})$ is obtained from the same sequence without the unitary in question $u_k(\alpha_k)$, i.e., $\prod_{t=0}^{k-1} u_t(\alpha_t) \cdot \prod_{t=k+1}^{T} u_t(\alpha_t)$. In other words: A unitary $u_k(\alpha_k)$ is unimportant if omitting it completely has only a small impact on the performance function, i.e., $\Phi(\boldsymbol{\alpha}) \approx \Phi^{\bar{k}}(\boldsymbol{\alpha})$. Thanks to Eq. (29), the calculation of $\Phi^{\bar{k}}(\boldsymbol{\alpha})$ is efficient.

b. Second criterion

We like to introduce a second criterion for a good sequence $\prod u_t(\alpha_t)$. In the experimental realization, it is favorable to deal with only one type of Mølmer-Sørensen (MS) gates $u_{\text{MS}} = \exp(-i \cdot \alpha_{\text{MS}} \cdot S_{x/y}^2)$, i.e., we like α_{MS} to be the same for all MS gates in the sequence. Further, the value of α_{MS} should be a natural fraction of π. Interestingly, this seems to be a favorable numerical value, as well. In the best sequences $\prod u_t(\alpha_t)$ we found for various U_{target}, all α_t (not just the α_{MS}) turned out to have quantized values of the type $\alpha_t = \frac{m_t}{2^{n_t}} \cdot \pi$, with $m_t \in \mathbb{Z}$, $n_t \in \mathbb{N}_0$. Therefore, including side conditions which favor such values also allows us to improve the optimization process.

2. Optimization

The performance function might be optimized by various standard optimizers. As already pointed out in Sec. III D, the product structure of the performance function allows an efficient calculation of its gradient such that one might choose a method such as, e.g., GRAPE [10], which takes advantage of this information. Still, we favored an alternative approach, which optimizes all α_t individually based on a second-order Taylor expansion. Due to its simple nature, this algorithm can be easily altered and therefore allows a neat integration of the extra criteria formulated in the last section, as we demonstrate below.

Except for trivial problems, the numerical maximization of the performance function consists of many optimization cycles, where all α_t are adjusted repeatedly. To optimize one specific parameter α_k, all other parameters $\alpha_0, \alpha_1, \ldots, \alpha_{k-1}, \alpha_{k+1}, \ldots \alpha_T$ are kept constant mapping the multivariable function $\Phi(\boldsymbol{\alpha})$ to a single-variable function $\phi_k(\alpha_k)$,

$$\Phi(\boldsymbol{\alpha}) \equiv \Phi(\alpha_0, \alpha_1, \ldots \alpha_T) \to \phi_k(\alpha_k). \tag{B2}$$

The different parameters α_k are updated sequentially, starting with $k = 0$. Hereby, we take

advantage of the method described in Sec. III D. To use Eq. (29) we need to know the expressions $\langle f_{lj}|\prod_{t=0}^{k-1} u_t(\alpha_t)$ and $\prod_{t=k+1}^{T} u_t(\alpha_t)|i_{lj}\rangle$ for each k. The actual $\langle f_{lj}|\prod_{t=0}^{k-1} u_t(\alpha_t)$ can be derived from its predecessor $\langle f_{lj}|\prod_{t=0}^{k-2} u_t(\alpha_t)$ after α_{k-1} has been updated, while all $\prod_{t=k+1}^{T} u_t(\alpha_t)|i_{lj}\rangle$ are ideally calculated iteratively at the beginning of each optimization cycle.

With this preparation, we can use Eq. (29) and its obvious generalizations to compute ϕ_k and its first and second derivative ϕ_k', ϕ_k'' at the current value of α_k. This allows us to approximate ϕ_k by a parabola $\mathcal{P}_k$. The possibility to provide individual parabola approximations $\mathcal{P}_k$ for all α_k without great effort is actually one of the nice features of this simple optimization method.

If our sole objective was to maximize $\Phi(\boldsymbol{\alpha})$, the obvious choice would be $\alpha_k^{[\mathrm{new}]} = \alpha_k^{[\mathrm{max}]}$, where $\alpha_k^{[\mathrm{max}]}$ is the position of the maximum of the parabola,

$$\mathcal{P}_k(\alpha_k^{[\mathrm{max}]}) = \max\left(\mathcal{P}_k(x)\right). \tag{B3}$$

This should be backed up by some security protocols in case $\mathcal{P}_k$ turns out to have positive curvature, $\max\left(\mathcal{P}_k(x)\right) = \infty$ or the estimated function value is far off the real value $|\phi_k(\alpha_k^{[\mathrm{new}]}) - \mathcal{P}_k(\alpha_k^{[\mathrm{new}]})| \gg \varepsilon$. Since we also have to keep the criteria in mind that we formulated in the last Sec. B 1, we introduce a slightly altered procedure.

a. *First criterion*

The first criterion states the preference of solutions where as many α_k as possible have turned into zero. Since we do not possess a priori knowledge which or how many α_k should become zero, this criterion can not be phrased as an equation which has to be fulfilled during the entire optimization.

A feasible way is to add an adaptable potential $\Lambda(\boldsymbol{\alpha})$ to the performance function and maximize the sum $\Phi(\boldsymbol{\alpha}) + \Lambda(\boldsymbol{\alpha})$. The potential $\Lambda(\boldsymbol{\alpha})$ has to be designed such that it drags the α_k of the less important unitaries $u_k(\alpha_k)$ towards zero. In this fashion, the few important $u_k(\alpha_k)$ are urged to compensate for the less important ones and finally replace them. At the end of the entire optimization procedure, when only few $\alpha_k > 0$ have survived, $\Lambda(\boldsymbol{\alpha})$ must be set to zero such that a pure maximum of $\Phi(\boldsymbol{\alpha})$ can be reached.

Instead of designing potentials $\Lambda(\boldsymbol{\alpha})$, we can also go a much more direct way and simply set

$$\begin{aligned} \alpha_k^{[\mathrm{new}]} &= \alpha_k^{[\mathrm{max}]} - \delta_k^{[0]} \\ &\text{with } |\delta_k^{[0]}| \leq |\alpha_k^{[\mathrm{max}]}|;\ \mathrm{sign}(\alpha_k^{[\mathrm{max}]}) = \mathrm{sign}(\delta_k^{[0]}). \end{aligned} \tag{B4}$$

Obviously, $\delta_k^{[0]}$ pushes $\alpha_k^{[\mathrm{new}]}$ closer towards zero but also prevents the sequence from fully maximizing the performance function Φ. Therefore, the $\delta_k^{[0]}$ have to be adopted during the optimization process, as described for the potential $\Lambda(\boldsymbol{\alpha})$. So, what is the correct size of the $\delta_k^{[0]}$? First, it should be noted that for each optimization step the omitted improvement of the performance function due to the displacement $\delta_k^{[0]}$ can be obtained as

$$\begin{aligned} \Delta_k^{[0]}\Phi(\delta_k^{[0]}) &= \phi_k(\alpha_k^{[\mathrm{max}]}) - \phi_k(\alpha_k^{[\mathrm{new}]}) \\ &= \phi_k(\alpha_k^{[\mathrm{max}]}) - \phi_k(\alpha_k^{[\mathrm{max}]} - \delta_k^{[0]}). \end{aligned} \tag{B5}$$

The value of the omitted improvement $\Delta_k^{[0]}\Phi(\delta_k^{[0]})$ can also be estimated with the help of the approximation parabola $\mathcal{P}_k$

$$\Delta_k^{[0]}\Phi(\delta_k^{[0]}) \approx \mathcal{P}_k(\alpha_k^{[\mathrm{max}]}) - \mathcal{P}_k(\alpha_k^{[\mathrm{max}]} - \delta_k^{[0]}). \tag{B6}$$

The decisive advantage of this approximation is that it is easy to invert. This allows us to proceed as follows: We decide which omitted improvement $\Delta_k^{[0]}\Phi(\delta_k^{[0]})$ we are willing to tolerate and with this value we directly infer the corresponding displacement $\delta_k^{[0]}$. In case we get $|\delta_k^{[0]}| \geq |\alpha_k^{[\mathrm{max}]}|$, we include the (non-analytic) rule to set $\alpha_k^{[\mathrm{new}]} = 0$ and erase the unitary $u_k(\alpha_k)$ from the sequence.

Hence, the new question arises: What do we choose as tolerable $\Delta_k^{[0]}\Phi$? Following Sec. B 1, $\Delta_k^{[0]}\Phi$ should be chosen as a reciprocal function of the importance $I[u_k(\alpha_k^{[\mathrm{max}]})]$ (B1). Just to give an example (not as exclusive choice), in our calculations we frequently used

$$\Delta_k^{[0]}\Phi = \gamma^{[0]} \cdot \left[\left(\frac{0.25}{I[u_k(\alpha_k^{[\mathrm{max}]})]}\right)^5 + 1\right]. \tag{B7}$$

The coupling factor $\gamma^{[0]}$ is adapted according to the stage of optimization: At the very beginning, the system needs some optimization time to get close enough to the maximum to develop a preliminary hierarchy of important and unimportant unitaries in the sequence $\prod_t u_t(\alpha_t)$. Hence, $\gamma^{[0]}$ starts very low in the beginning and gradually increases during the optimization. This increase often comprises many orders of magnitude. Only to the very end, when all unimportant unitaries have died away, $\gamma^{[0]}$ is set to zero to reach an undisturbed maximum of the performance function Φ.

The value of the coupling constant $\gamma^{[0]}$ directly influences the number of unitaries in the sequence. If this number is reduced too quickly, there might not be sufficient degrees of freedom left to reach the maximum, while too many unimportant unitaries in the sequence might prove fatal as well, since they tend to suffocate the optimization. Any protocol used to adjust $\gamma^{[0]}$ should find the right balance between these two situations.

b. *Second criterion*

The second criterion formulated in Sec. B 1 favors quantized values $\alpha_k = \frac{m_k}{2^{n_k}} \cdot \pi$, with $m_k \in \mathbb{Z}$, $n_k \in \mathbb{N}_0$.

With slight modification, this criterion can be enforced with a similar method as used to drag the α_k towards zero. First, we replace $\delta_k^{[0]}$ in Eq. (B4) by a new displacement $\delta_k^{[\text{quant}]}$ which pushes $\alpha_k^{[\text{new}]}$ towards the quantized value $\frac{m_k}{2^{n_k}}\pi$ which is next to $\alpha_k^{[\text{max}]}$. The replacement of $\delta_k^{[0]}$ by $\delta_k^{[\text{quant}]}$ is most usefully performed towards the end of the optimization process, when $\delta_k^{[0]}$ has done most of its job and the number of unitaries in the sequence is already strongly reduced. Analog to $\delta_k^{[0]}$, the displacement $\delta_k^{[\text{quant}]}$ is derived from a pre-defined $\Delta_k^{[\text{quant}]}\Phi$ (B6). While the strength of $\Delta_k^{[0]}\Phi$ is calculated using the importance $I[u_k(\alpha_k^{[\text{max}]})]$ (B7), there is no particular reason to do so for $\Delta_k^{[\text{quant}]}\Phi$. It seems more meaningful to relate the value of $\Delta_k^{[\text{quant}]}\Phi$ to the proximity of $\alpha_k^{[\text{max}]}$ to the next quantized value. That is, $\Delta_k^{[\text{quant}]}\Phi$ is set to zero if $\alpha_k^{[\text{max}]}$ is placed in the middle between two quantized values and increases when $\alpha_k^{[\text{max}]}$ approaches one of them.

To avoid false expectations, it should be mentioned that finding solutions where all α_k are nicely quantized is supported by the described method but not guaranteed. Using a multi-ansatz with many different initial sequences is still a key element to success.

For the Mølmer-Sørensen (MS) gates, we actually use a far more drastic approach. Since we favor solutions with only one type of MS gates $u_{\text{MS}} = \exp(-i \cdot \alpha_{\text{MS}} \cdot S_{x/y}^2)$, it turned out to be advantageous to fix their number and their α_{MS} already in the initial sequence $\prod u_t(\alpha_t^{\text{inital}})$ and never allow the computer to change these values during the optimization. Of course, this obliges us to optimize over different types of initial sequences, but we found that the improvements gained in the optimization compensate by far for this little inconvenience.

c. *Simulated annealing*

Numerical algorithms based on stepwise local optimization often face the problem that they get stuck in local extrema. Algorithms built on simulated annealing [20] try to avoid this problem by accepting locally suboptimal moves too, albeit with a reduced probability. To incorporate an analog effect, one might introduce a third displacement $\delta_k^{[\text{sim. anneal.}]}$ stemming from $\Delta_k^{[\text{sim. anneal.}]}\Phi$ which is randomly drawn from an adequate Boltzmann distribution. By adapting $\Delta_k^{[\text{sim. anneal.}]}\Phi$, we can tune the algorithm continuously between an optimal local search and simulated annealing. Further, this algorithm never does an optimization in vain, contrary to "classical" simulated annealing, where certain results are rejected with a probability depending on the outcome.

Alternatively, the system can be disturbed and pushed out of a local extremum by a variation of the coupling factors $\gamma^{[0]}$ and $\gamma^{[\text{quant}]}$. Probably the most powerful method to escape a local trap is to complement the sequence $\prod u_t(\alpha_t)$ with new unitaries $u_{\text{new}}(\alpha \approx 0)$ close to the identity. Of course, this method must be handled wisely, since it counteracts the first criterion, which favors short sequences.

3. Protocols

The optimization algorithm described above contains the open parameters $\gamma^{[0]}$ (B7) and $\gamma^{[\text{quant}]}$, $\gamma^{[\text{sim. anneal.}]}$ (not explicitly mentioned) to adjust $\Delta_k^{[0]}\Phi$, $\Delta_k^{[\text{quant}]}\Phi$, and $\Delta_k^{[\text{sim. anneal.}]}\Phi$. Hence, we need a protocol telling us how these parameters should be adopted according to the stage of the optimization process. Unfortunately, it is neither straightforward to fathom the stages nor to associate them with precise values for the parameters. We spent a considerable amount of time to develop a good heuristic which does this job, but most of it is based on intuition and only few on scientific facts. Therefore, we do not deem it appropriate to go into any greater detail here.

Still, one further optimization protocol is worth mentioning: The optimization routine we have described so far starts with a random sequence and tries to end up with a sequence $\prod_t u_t(\alpha_t)$ which reproduces the target operation U_{target} (up to a gauge transformation). Once we have found such a sequence and saved it to the disk, we might wish to go on optimizing it and, e.g., try to find a shorter solution. Here, the problem is that each solution is already a maximum of the performance function and therefore the optimization gets stuck in a local trap.

a. *Disturbing the sequence*

To escape such a trap, the algorithm has to be disturbed. While the methods described in Sec. B 2 c tend to disturb the sequence everywhere a little bit, we found it more promising to introduce a few strong local disturbances. The motivation for this approach roots in the observation that improvements – even those obtained with other means – often affect only very few unitaries in the sequence and leave the rest unchanged.

In concrete terms, the procedure looks as follows: We start with the perfect sequence $\prod_t u_t(\alpha_t)$ and choose one unitary $u_k(\alpha_k)$ by random. This unitary is either replaced by $u_k(\alpha_k) \to u_k(-\alpha_k)$ or by $u_k(\alpha_k) \to u_k(0)$ (choice by random). If the algorithm is able to restore the sequence, we repeat the procedure with the same disturbance plus one more. This is done until the algorithm fails to repair the damage. Then, the sequence is filled up with (lots of) fresh unitaries $u_{\text{new}}(\alpha \approx 0)$ and optimized once more. If no improvement has been found until now, we start again with the perfect sequence $\prod_t u_t(\alpha_t)$ and a new single disturbance.

We like to point out that this approach might become of greater importance in future applications, when quan-

tum algorithms reach a complexity where solutions can no longer be found by ab initio methods. In this case, solutions have to be assembled from solutions of solvable subproblems. These assembled solutions are also maxima of the performance function but might still be optimizable with the procedure described above. An example for such an approach can be found in the Results Sec. IV B 2, where the assembled solution of the joint measurement of all four stabilizers of the five qubit code allowed for quite a successful optimization, which reduced the original assembled solution consisting of 52 unitaries to a solution comprising only 30 unitaries.